

*Department of Civil Engineering,
University College,
Cork.*



Observations and Modelling of Carbon Dioxide flux from an Irish Grassland for a one year campaign

By

Charlotte Le Bris

*A Thesis submitted to the National University of Ireland
In part candidature for the Degree of Master of Engineering Science*

October 2002

To my Family

Acknowledgements

The author wishes to express his thanks to the following people:

Prof. Ger Kiely, my supervisor, for his guidance and his encouragements.

Prof. Gabriel Katul, Prof. Ram Oren and Prof. John Albertson, from Duke University for their helpful advice.

Prof. J.P.J. O' Kane for use of the facilities of the Department of Civil Engineering, U.C.C.

Dr. Michael Creed, for his enthusiasm for international relationships

Yan Lacaze, Fidelma Horgan and Dermot Moynahan for their permanent help, and friendship.

Brendan Keenan, for his help and encouragements for my coming in Ireland.

Cecile Delolme for her time and interest all along this year.

My family for their permanent telephonic supports and encouragements.

Abstract

Seasonal variations in the CO₂ flux were investigated and modelled over a grassland in South West Ireland. The climate is temperate and humid with mean annual precipitation of about 1400 mm for the area. The grassland type can be described as moderately high quality pasture and meadow classified into the C₃-grass category. Data were recorded continuously at 30 minutes intervals by an aerodynamic method for one full year, between the 3rd of July 2001 and the 3rd of July 2002. The grassland absorbed CO₂ during the periods from July to September 2001 and from February to July for 2002. The maximum daily net ecosystem CO₂ exchange during the growing period was up to 20 g of CO₂ m⁻² day⁻¹ and the net uptake for the whole period was 3.8 T of Carbon. Those results are compared with CO₂ fluxes for grasslands for other countries with different climates and land use management.

Two semi-empirical models were then applied to simulate the net ecosystem CO₂ flux. The model proposed by Collatz *et al* (1991) considers the full biochemical components of photosynthetic carbon assimilation from Farquhar *et al.* (1980), and an empirical model of stomata conductance from Ball *et al.* (1987). The model proposed by Jacobs (1994) is based on the empirical model of stomatal conductance from Jarvis (1976), and on a less detailed assimilation model from Goudriaan *et al.* (1985). Both models satisfactorily predict CO₂ fluxes over the seasons for the grass catchment.

Contents

Acknowledgements	iii
Abstract.....	iv
Table of Contents	v

Chapter 1	Introduction
------------------	---------------------

1.1 General Background.....	1
1.2 Methods.....	1
1.3 Objectives.....	2

Chapter 2	Data Acquisition
------------------	-------------------------

2.1 Site description.....	5
2.1.1 Location	5
2.1.2 Climate	6
2.1.3 Field history	7
2.2 Description of instruments and methods	8
2.2.1 Weather station.....	8
2.2.2 Wind speed and direction.....	9
2.2.3 Net Radiation.....	10
2.2.4 Photosynthetic photon flux or PAR (Photosynthetic Active Radiation).....	11
2.2.5 Soil heat flux	12
2.2.6 Latent heat flux and sensible heat flux.....	12
2.2.7 CO ₂ / H ₂ O fluxes	13
2.2.8 Soil moisture	16
2.2.9 Stream flow	16

Contents

Chapter 3

Data Analysis

3.1 General meteorological data	19
3.1.1 Global data.....	19
3.1.2 Precipitation and water balance	20
3.2 Momentum flux filter.....	21
3.3 CO ₂ Filter	23
3.3.1 Nighttime	23
3.3.2 Daytime	23
3.4 Gap filling function	23
3.4.1 Nighttime data.....	24
3.4.2 Daytime data	25
3.5 Six weeks gap filling.....	28
3.5.1 Site position method.....	28
3.5.2 Inverse Spring method	29
3.6 Corrections	30
3.6.1 Day length correction	30
3.6.2 Webb Correction	32
3.7 Final results and discussion.....	34
Site	39
References	40

Contents

Chapter 4

Modelling

4.1 Introduction	44
4.1.1 Global processes	44
Photosynthesis.....	44
Dark respiration	45
Photorespiration	46
Soil respiration	46
Plant categories	46
Stomata	46
4.1.2 Terminology	47
4.2 Models presentation.....	48
4.2.1 Collatz's Model.....	48
Assimilation	48
Temperature response	49
Stomatal conductance	49
4.2.2 Jacobs or A-g _s Model	50
Assimilation	51
Temperature response	52
Stomatal conductance	53
4.3 Calibration	54
4.3.1 Collatz's model	55
4.3.2 Jacobs' model.....	56
4.4 Modelling results and comparisons.....	58
4.4.1 Half-hour average flux	58
4.4.2 Daily flux	60
4.4.3 Monthly flux.....	60
4.4.4 Cumulative photosynthesis & global uptake	62
References	65

Contents

<u>Chapter 5</u>	<u>Conclusion</u>
5.1 Conclusion.....	66
5.2 Suggestions for future investigations.....	67
Bibliography.....	69
Appendix 1.....	74
Appendix 2.1.....	79
Appendix 2.2.....	82
Appendix 3: Complementary Production.....	85

Chapter 1

Introduction

1.1 General Background

In recent years, there has been considerable concern about possible climatic changes and increasing concentrations of atmospheric carbon dioxide. The International Panel on Climate Change (IPCC) estimated that the ambient CO₂ concentration might be doubled by the end of the next century (Houghton *et al.*, 1990). Needs to quantify the global carbon balance, as well as to understand the spatial and seasonal pattern of CO₂ flux led many studies investigating the carbon dioxide fluxes in oceanic and forest ecosystems. Less examined environments are grasslands. However, this ecosystem is a major component of the Earth's natural vegetation, especially in the Northern Hemisphere. In Ireland, approximately 50 % of the total landmass is lakes, mountains, bogs and the remaining 50% is made up of 5% cultivated field and 45% of grasslands. Several short-term studies have shown that grassland ecosystem can sequester atmospheric CO₂, but annual data is limited. So that long-term surface flux measurements are needed to quantify the source-sink potential of this particular environment (Ham & Knapp, 1998). These can then be used to elaborate and validate mechanistic models that describe the effects of the environment on biological functions and that can interpolate and predict the evolution of the current trend in term of carbon exchanges.

1.2 Methods

The location of the present study is a grazed grassland site in Southwest Ireland, very typical of the vegetation of this part of the country. The climate is temperate with a small range of temperature during the year and abundant precipitation. Several methods can be used to measure CO₂ fluxes. Here, CO₂ fluxes between the ecosystem and the atmosphere as well as other meteorological data were recorded continuously at 30 minutes intervals by an aerodynamic method over one full year (from July 2001 to July 2002). No device has been set up to measure specific soil respiration. Once collected, data were filtered and filled when found inadequate or suspect, as it is generally the case with tower-based flux measurements. Data were also lost during a six weeks period due to the power generator intermittent working (from Julian day 272 to 319 of year 2001). Missing sections of data were synthesized using empirical modelling, an approach that has been widely employed in similar studies (Falge *et al.*, 2001; Ham & Knapp, 1998).

From the basis of these data, a modelling module was calibrated. Two different semi-empirical models were tested in comparison with the measurements. On the one hand, the model proposed by Collatz *et al* (1991) considers the full biochemical components of photosynthetic carbon assimilation from Farquhar *et al.* (1980), and an empirical model of stomata conductance from Ball *et al.* (1987). On the other hand, the model proposed by Jacobs (1994), which is less demanding in inputs parameter and often linked with meteorological research (Calvet *et al.*, 1998).

It is based on the empirical model of stomatal conductance from Jarvis (1976), and on a less detailed assimilation model from Goudriaan *et al.* (1985). The calibration method applied was a sensitivity analysis for different time scale fluxes: 30 minutes averaged flux, daily flux, monthly flux and finally the global cumulative uptake over the year. Special attention was brought to the smallest time scale of 30 minutes for the choice in parameters. This flux is the most difficult to simulate because it really depicts the quick interactions of external parameters with plants. However it is believed here that good calibration for such a time step should bring satisfactory results for longer timescales.

1.3 Objectives

The aims of the present study are to determine the CO₂ flux over one year for a grassland in this temperate climate, and its main characteristics: seasonal variation, durations as a sink of carbon. Another issue is the analysis and comparison with other grassland sites, of the effects of meteorological and biological factors as well as land use management and climate on the exchange between grass and the atmosphere.

The modelling part of this work is just the first step of what could be achieved with such a tool. In this study, the models help to get a better understanding of processes at work, and try to give a faithful description of the reality. The comparison of two models is a good method to understand processes, and the level of complexity needed to fit CO₂ fluctuations.

Chapter 2

Data acquisition

Table of Content

2.1 Site description	5
2.1.1 Location.....	5
2.1.2 Climate	6
2.1.3 Field history.....	7
2.2 Description of instruments and methods.....	8
2.2.1 Weather station.....	8
2.2.2 Wind speed and direction.....	9
2.2.3 Net Radiation	10
2.2.4 Photosynthetic photon flux or PAR (Photosynthetic Active Radiation)	11
2.2.5 Soil heat flux.....	12
2.2.6 Latent heat flux and sensible heat flux	12
2.2.7 CO ₂ / H ₂ O fluxes.....	13
2.2.8 Soil moisture	16
2.2.9 Stream flow.....	16

2.1 Site description

2.1.1 Location

The grassland of this study is located in South West Ireland (see figure 2.1), 25 km northwest of the city of Cork (52° North latitude, 8° 30' W longitude).



Figure 2.1: The site area is located on this map of Ireland by the red dot

The 15 Ha research field is a headwater of the 84 km² Dripsey catchment, at an elevation of 195 m above sea level, with a gentle slope of 3 % grade (see figure 2.2). The soil profile includes a top layer (5-10cm thick) of humus over a sandy loam subsoil layer of 45 cm thick. The grassland type can be described as moderately high quality pasture and meadow.



Figure 2.2: Field of study

2.1.2 Climate

The climate is temperate and humid with mean annual precipitation of about 1400 mm at the site. The rainfall regime is characterized by long duration events of low intensity (values up to 50 mm/day). Short duration events of high intensity are more seldom and occur in summer. It can be seen on figure 2.3 that the year of the study (July 2001- July 2002) was especially wet with already 873.2 mm in five months in 2002 and a much steeper slope than the previous years for that period. Daily air temperatures have a very small range of variation during the year, going from a maximum of 23° C to a minimum of 0° C., with an average of 15° C. in summer and 5° C. in winter. No air frost has been noticed during the study period. This part of Ireland is windy with a mean wind velocity of 16 km/h at the site with peaks up to 60 km/h. The wind comes from the west 40 % of the time.

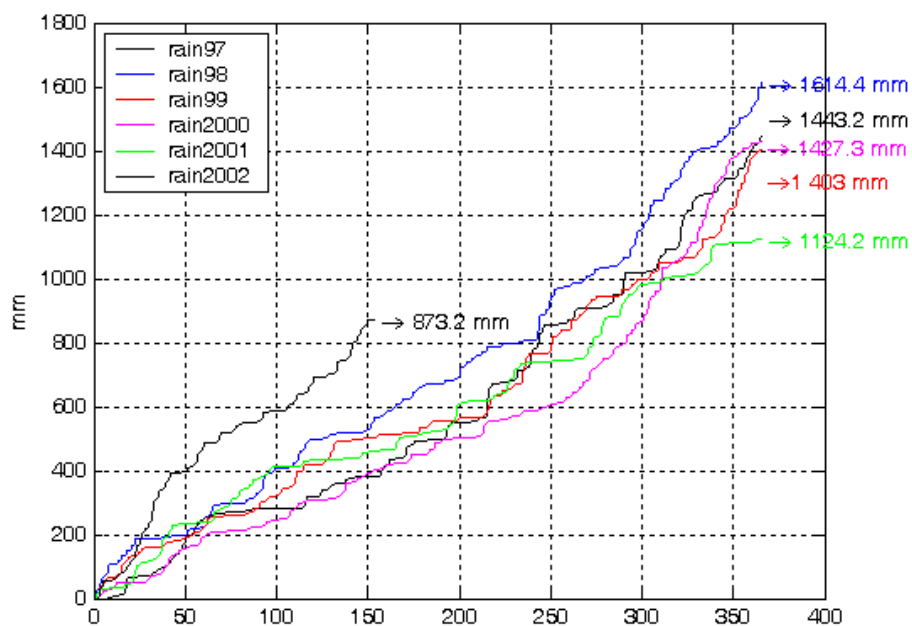


Figure 2.3: Cumulative precipitations in mm from January to December in 1997, 98, 99, 200,2001,and from January to June 2002.

2.1.3 Field history

The 15 Ha grassland field is highly nitrogen fertilized (about 450 kg of Nitrogen /Ha/yr), grazed in autumn and spring and the grass is cut as silage twice a year in summer. Figure 2.4 gives a good understanding of the field history between May 2001 and July 2002.

In 2001, the grass was cut in May the 20th, as silage, and July the 10th, as hay, and removed from the fields. The grazing periods are not continuous on one field but they last one week every three or four weeks, since cattle move from one pasture to another. The autumnal grazing period is about five months long from July to December whereas the spring one is usually two months long. The height of grass just before cutting in summer is about 0.5 m, whereas it is down to 0.15 m in wintertime during the resting period. This later stage lasts two months when, thanks to the climatic conditions, the field stays green.

Considering the environmental conditions (warm but not hot temperatures, high humidity with very good airflow) and the medium latitude of Ireland, the metabolic pathway for carbon fixation is assumed to be a Calvin-Benson Cycle (C₃ Cycle grass category in Chapter 4).

Up to now (September 2002), no measurement of the biomass or of the Leaf Area Index (LAI) of grass has been made on this site. As far as those quantities are concerned, we will use all along this study general Irish values given by H. Tunney from the Johnstown Castle Research Centre (personal communication). For such a grassland field with similar field history, the biomass is considered to be:

Biomass < 1 T of Dry Matter /ha during the resting period in winter
 up to 4 or 5 T of Dry Matter /ha in summer before silage
 from 1 to 2 T of Dry Matter /ha during grazing
 and typically up to 12 T of Dry Biomass /ha/year

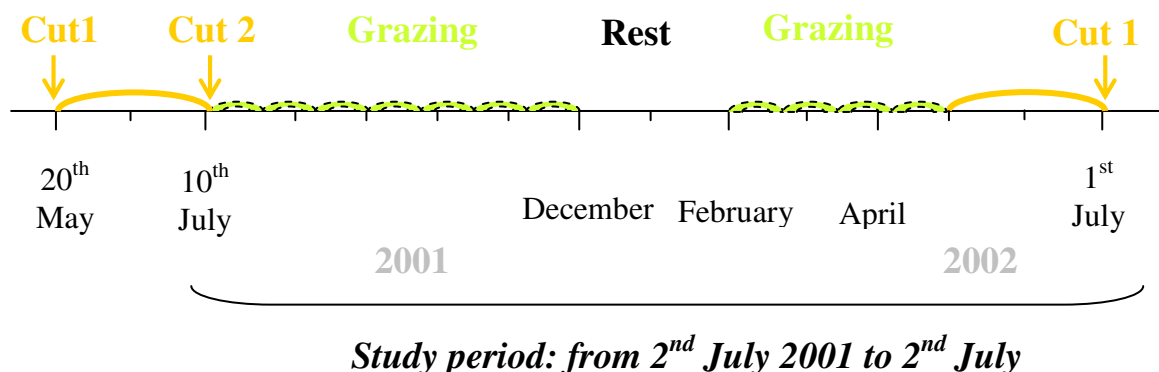


Figure 2.4: Field history diagram for the study period from July 2001 to July 2002

2.2 Description of instruments and methods

In this part, an overview of the sensors and techniques used for the data collection is given. First, a general weather station will be described, followed by a detailed look at the main meteorological data devices.

2.2.1 Weather station

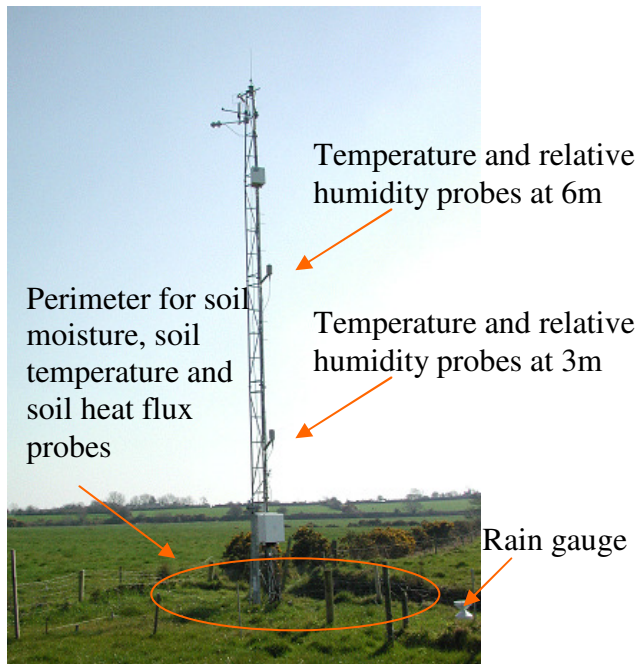


Figure 2.5: Tower in full height, 10 m.

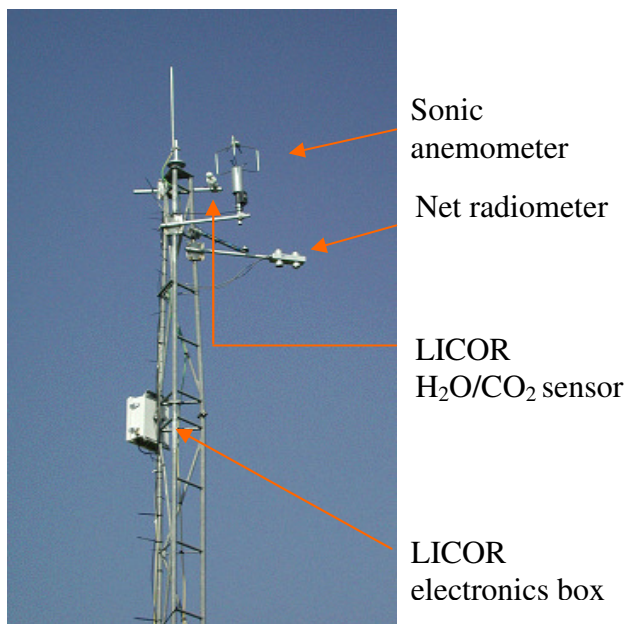


Figure 2.6: Top of the tower with instruments

A typical automatic weather station consists of a set of weather sensors connected to a datalogger, which controls the measurements, the data processing and the digital storage of the sensor outputs.

The experimental system, in this study, is composed of a 10 m high tower, which supports the different types of sensors. A secured perimeter has been defined with a wire fence to protect the tower sensors, as well as to define a setting up area for the soil devices (see figure 2.5).

Figure 2.5 shows the tower in its full height. It identifies the positions of the relative humidity and air temperature sensors at 6 m and 3 m, the rain gauge on the ground, and the soil moisture, soil heat flux plates and soil temperature probes underground. The white box near the foot of the tower is called ‘Campbell environmental box’ and houses the datalogger, the multiplexer, the barometric pressure sensor, as well as a modem telephone connection. Figure 2.6 focuses on the top of the tower, showing the position of the net radiometer, the sonic anemometer, and the CO₂/H₂O gas analyser.

Table 2.1 lists the sensors and logging equipments used for the data collection.

Logging devices	<ul style="list-style-type: none"> • 1 Datalogger • 1 Multiplexer • 1 modem telephone connection 	<ul style="list-style-type: none"> • CR23X from Campbell sc. • AM 16/32 from Campbell sc.
Sensors	<ul style="list-style-type: none"> • 1 Net radiometer • 1 3D Sonic anemometer • Combined humidity & temperature probes • 1 Barometric pressure sensor • 1 CO₂/H₂O gas analyser • 1 PAR sensor • Soil heat flux plates • Soil temperature probes • 6 Soil moisture monitors • 1 Rain gauge 	<ul style="list-style-type: none"> • CNR 1 from Kipp & Zonen • Model 8100 from RM Young • HMPC45C from Campbell sc. • PTB101B from Campbell sc. • LI-7500 from Licor • PAR LITE from Kipp & Zonen • HFP01 from Campbell sc. • Model 107 from Campbell sc. • CS615 from Campbell sc. • ARG100

Table 2.1: Equipment employed for the study

2.2.2 Wind speed and direction

We utilized the model 8100 sonic anemometer from RM Young to perform wind velocity and wind direction measurements at 10 Hz. It makes observations of the wind velocities by measuring the travel time of ultrasonic signals sent between the upper and lower transducers (see figure 2.7). By measuring the transit time in each direction along all three paths, the three dimensional wind velocity and speed of sound may be calculated. The sonic temperature is derived from speed of sound



Figure 2.7: the sonic anemometer with the three paths shown in red (E -W), blue (SW-NE), green (NW-SE), as for a typical orientation of the device

2.2.3 Net Radiation

The net radiometer used here is a CNR1 net radiometer from Kipp & Zonen. It is intended to analyse the radiation balance of Solar and Far Infrared radiation. The most common application is the measurement of Net Radiation at the earth's surface. Solar radiation is measured thanks to two pyranometers. One facing upward, measures incoming radiation from the sky, and the other, which faces downward, measures the reflected Solar radiation (see figure 2.8). Thus the albedo (α), which is the reflection coefficient of solar radiations for a particular ground surface, can also be determined.

$$\alpha = \frac{(\text{reflected solar radiations})}{(\text{incoming solar radiations})} \quad (2.1)$$

Far infrared radiation is measured by means of two pyrgeometers. One facing upward, measures the far infrared radiations from the sky, the other, which faces downward, measures far infrared radiations from the soil surface (see figure 2.8).



Figure 2.8: Net radiometer and its main components

Operational overview:

A pyranometer consists in a thermopile sensor, a housing, a glass dome and a cable. The thermopile is coated with a black absorbent paint, which absorbs the radiations and converts them into heat. The resulting heat flow causes a temperature difference across the thermopile. The thermopile generates a voltage output. The absorber paint and the dome determine spectral specifications. The thermopile is encapsulated in the housing in such a way that its field of view is 180° degrees, and that is angular characteristics fulfil the so-called cosine response. The conversion from voltage (V) into solar irradiance (incoming or reflected) in W/m² is a constant calibrated factor (C).

$$E = \frac{V}{C} \quad (2.2)$$

A pyrgeometer consists of a thermopile sensor, a housing, and a silicon window. The thermopile works the same way as for the pyranometer. The window serves both as environmental protection and as a filter. It only transmits the relevant far infrared radiation, while obstructing the solar radiation. The thermopile is encapsulated in its housing, so that its field of view is 150 degrees, and its angular characteristics fulfil the so-called cosine response as much as possible, in this field of view. The limited field of view does not produce a large error because the missing part of the field of view does not contribute significantly to the total, and is compensated for during calibration. The pyrgeometer temperature (T) is needed for estimating the far infrared radiation from the voltage (V). Hence, a temperature sensor is located in the net radiometer body. The calculation of far infrared irradiance (E) in W/m^2 is given hereunder:

$$E = \frac{V}{C} + 5.67 \times 10^{-8} \times T^4 \quad (2.3)$$

The calculation of the net total radiation is performed automatically by the device and is thus given in as an output in W/m^2 :

$$NR = E_{\text{incoming solar}} + E_{\text{far infrared from sky}} - E_{\text{reflected solar}} - E_{\text{far infrared from ground}} \quad (2.4)$$

2.2.4 Photosynthetic photon flux or PAR (Photosynthetic Active Radiation)

The photosynthetic photon flux can be easily calculated with the incoming solar radiations, given some approximations:

- the energy content of photons is the same for all wave length. It is equal to the energy content of photons at the mean wave length of the spectrum (green, 0.55 μm) that is $3.6 \cdot 10^{-19}$ J/photon (=0.217 J/ μmol).
- about 45% of the incoming solar radiations are in the PAR wave length.

Then,

$$Q_{PAR} = \frac{0.45 \times E_{(inco min gsolar)}}{0.217} = \frac{W}{m^2} \times \frac{\mu mol}{J} = \frac{\mu mol}{m^2 \times s} \quad (2.5)$$

In order to avoid those approximations, a sensor was used for the photosynthetic flux: PAR LITE from Kipp & Zonen. It has not been used from the beginning of the study period but from November 2001. Thus for the early period, Q_{par} was calculated as explained above. PAR LITE uses a photodiode sensor, which creates a voltage output that is proportional to the incoming radiation from the entire hemisphere. A special optical filter has been designed to provide a quantum response in the photosynthetically active radiation (PAR) (between 0.4 and 0.7 μm). The output, photosynthetic photon flux, is given in $\mu mol/m^2.s$

2.2.5 Soil heat flux

Soil heat flux is often ignored because its magnitude is very small, compared to the other terms of the energy balance equation (about 10% of the net radiation). However it is an important parameter to determine evaporation of water. It has been monitored here, thanks to heat flux plates HFP01 from Campbell scientific. Typically, two sensors are buried in the ground around a meteorological station at a depth of 20mm below the surface.

A sensor is based on a thermopile, a number of thermocouples connected in series, placed in a material acting like a thermal resistance. When heat is flowing through the sensor, a temperature gradient takes place flowing from the hot to the cold side of the sensor. Thermocouples then generate an output voltage that is proportional to the temperature difference between its ends. Using more thermocouples in series will enhance the output signal.

2.2.6 Latent heat flux and sensible heat flux

Neglecting the less important terms such as heat storage and energy absorbed by physiological processes, the energy balance at the surface is given by:

$$R_{net} = G + H + \lambda E \quad (2.6)$$

Where R_{net} (W/m^2) is net radiation given by the net radiometer, G (W/m^2) is the ground heat flux given by heat flux plates, H (W/m^2) is the sensible heat flux and λE (W/m^2) is the latent heat flux. Those two later components are not measured directly by any device, but calculated using the eddy correlation technique with air temperature and air specific humidity (using the LICOR and the sonic anemometer).

Horizontal momentum of the air is transferred toward the ground where it is dissipated in frictional drag. Energy is transferred from larger eddies aloft downward to smaller eddies by turbulent mixing. The eddy velocities are departures from a characteristic mean. Thus, in a turbulent atmosphere, the instantaneous vertical transport of some atmospheric constituent is given by the product of the fluctuation of the concentration with the fluctuation of the vertical wind velocity.

Considering the vertical velocity component of the wind vector, w (m/s), the instantaneous velocity can be written as the sum of the average velocity and a turbulent part (Reynolds averaging):

$$w = \bar{w} + w' \quad (2.7a)$$

The turbulent eddies from the specific humidity and temperature can be separated exactly the same way. Turbulent fluctuations in specific humidity are written as q' , and the turbulent part of the instantaneous temperature is T' .

$$q = \bar{q} + q' \quad T = \bar{T} + T' \quad (2.7b\&c)$$

By definition, the average value of the turbulent parts of the velocities and scalars equals zero: $\bar{w}' = \bar{q}' = \bar{T}' = 0$.

Since the site is horizontally uniform, and atmospheric conditions are assumed steady over the averaging period (30 minutes), it is expected that: $\overline{w} = 0$

The wind velocity may be written as a volume flux. Then the product of the vertical volume flux w (m/s), and the density of moist air ρ_a (kg/m³), is the mass flux of moist air, $\rho_a w$ (kg/m²/s). With q the relative humidity and λ the latent heat of vaporization, the latent heat flux can be written $\lambda \rho_a w q$ (W/m²). The mass flux of air may be related, as well, to a specific property of the air such as the specific heat per unit mass, $c_p T$ (J/kg), to give the sensible heat flux $\rho_a w c_p T$ (W/m²) with c_p the specific heat capacity of moist air in J/kg/K.

Considering the atmospheric density as constant for the lower part of the atmospheric boundary layer ($\rho_a = 1.29$ kg /m³), and applying Reynolds averaging to the property flux, the average flux of a constituent X can be written :

$$\overline{\rho_a w X} = (\overline{\rho_a} + \overline{\rho_a'}) (\overline{w} + \overline{w'}) (\overline{X} + \overline{X'}) = \rho_a \overline{w' X'} \quad (2.8)$$

Then the average latent heat flux becomes:

$$\lambda E = \lambda \rho_a \overline{w' q'} \quad (2.9)$$

And the average sensible heat flux

$$H = \rho_a \overline{w' (c_p T)'} \quad (2.10a)$$

This equation is often simplified, considering c_p as constant ($c_p = 1005$ J/kg/° K):

$$H = \rho_a c_p \overline{w' T'} \quad (2.10b)$$

2.2.7 CO₂ / H₂O fluxes



Figure 2.9: LI-7500 Open path CO₂/H₂O gas analyser

A LI-7500 Open Path CO₂/H₂O non-dispersive, absolute infrared gas analyser, has been chosen to measure carbon dioxide and water vapor densities in the turbulent air. In the eddy covariance technique, these data are used in conjunction with sonic anemometer air turbulence data to determine the fluxes of CO₂ and H₂O. A high frequency sonic anemometer (10 Hz) and high precision analyser such as LI-7500 is needed to correctly sample the turbulent eddies in the lower boundary layer. The sensor head has a smooth, aerodynamic profile, in order to minimize flow disturbance.

In the eddy correlation method, the flux, F_c of gas is given by:

$$F_c \cong -\overline{w' \rho_c'} \quad (2.11)$$

Where c' is the density fluctuation of gas c (mol/m³), measured with the LI-7500, and w' is the vertical wind velocity fluctuations (m/s), given by the sonic anemometer.

The open path analyser eliminates time delays, pressure drops, and sorption/desorption of water vapor on tubing employed with a closed path analyser.

The LI-7500 is placed close to and within about 20 cm of the centroid of the air volume measured by the sonic anemometer.

Operational overview:

The LI-7500 sensor head has a 12.5 cm open path, with single-pass optics and a large 1 cm diameter optical beam. The LI-7500 operates over a temperature range of -25 to +50 °C. Figure 2.10 shows a cutaway representation of the LI-7500 sensor head. The **Infrared Source** emits radiation, which is directed through a **Chopper Filter Wheel**, **Focusing Lens**, and then through the measurement path to a cooled **Lead Selenide Detector**. Focusing the radiation maximizes the amount of radiation that reaches the detector in order to provide maximum signal sensitivity. The detector operates approximately as a linear quantum counter; that is, over much of its range the detector signal output v is proportional to the number of photons reaching the detector. The existence of certain gas on the IR path reduces the photon flux reaching the other side. Each absorbing gas reacts at different wavelength of photon. Absorption at wavelengths centered at 4.26 μm and 2.59 μm provide for measurements of CO_2 and water vapor, respectively. Reference filters centered at 3.95 μm and 2.40 μm provide excellent rejection of IR radiation outside the desired band, allowing the analyzer to reject the response of other IR absorbing gases. Source and detector lifetimes are greater than 20,000 hours. A **brush less Chopper Motor** rotates the chopper wheel at 9000 rpm. The windows at both ends of the optical path are made of sapphire, which is extremely hard and starch resistant, allowing for worry-cleanup of dirt and dust accumulation.

Calibration:

The LI-7500 is an absolute gas analyser, which means that the reference set during the calibration is a CO_2 free sample. The CO_2 molar density ρ_c (mmol/m^3) is a non-linear function of the difference between the calibrated signal v_{sample} (zero gas) and the signal generated by the detector when it performs measurements $v_{\text{calibrated}}$. The ratio, $v_{\text{calibrated}}/v_{\text{sample}}$ gives the ratio of photon flux in the presence of CO_2 and in its absence, which is just its transmittance τ . The absorbance A is simply $1 - \tau$. P_{cc}

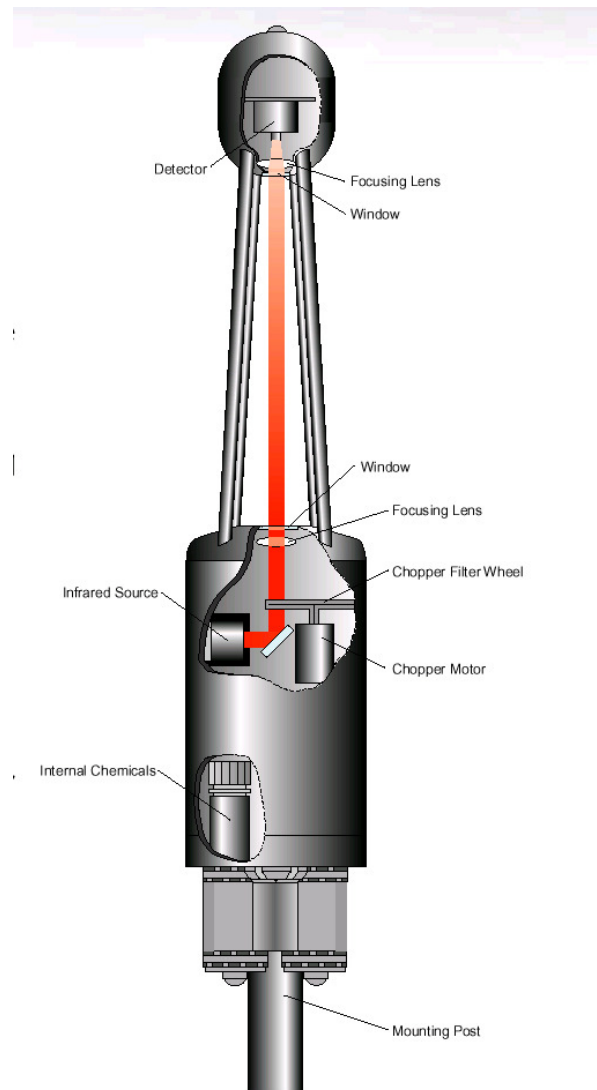


Figure 2.10: Cutaway representation of the LICOR (From LICOR manual)

represent the equivalent pressure of CO₂, S_c the span adjustment term and z_c the zeroing term.

$$\rho_c = P_{ec} \times f_c \left(\left[1 - \frac{v_{sample}}{v_{calibrated}} \times z_c \right] \times \frac{S_c}{P_{ec}} \right) = P_{ec} \times f_c \left(\frac{A \times S_c}{P_{ec}} \right) \quad (2.12)$$

The first calibration, the factory calibration, consists of determining the values of the calibration coefficients to describe this function f . A series of thirteen working calibration gases ranging in concentration from zero to 3,000 ppm are used. Factory calibration coefficients are obtained from a 5th order polynomial fit to the entire range of concentration from zero to 3,000 ppm. The nominal accuracy of the polynomial fit across the entire range of concentrations is about 1%. For water vapor, the calibration is similar except that fifteen data points between 0°C and 40°C dewpoint are used during the procedure to determine a third order polynomial (from LICOR manual).

The second step of the calibration as to be done just before using the sensor and consists in setting the analyser zero (z_c) and span (S_c). It is recommended to check the calibration after several months of use. The zero and span settings make the analyser's response agree with its previously determined factory response at least at two points. The LICOR was purchased in April 2001. It was first used in June 2001 and the first calibration was in November 2001. The results of the November calibration were as follows. We calibrated with a zero gas and a span gas of 543 ppm gas. Figure 2.11 shows that z_c and S_c were not well adjusted first, since the reading concentration of 0 ppm and 543 ppm were read by the LICOR as 8.11 ppm and 540 ppm respectively. However one can notice that in the measurement area, which is around the atmospheric concentration (about 380 ppm), the calibration has a very small impact on the measurements. When used for such measurements, the instrument is not very sensitive to the setting of z_c and S_c . An error in the span of the analyser wouldn't have enough impact to bias measurements. Consequently, measurements of CO₂ concentration taken between June and November has been considered as reliable, and has been used for the data analysis and model calibration parts of this study.

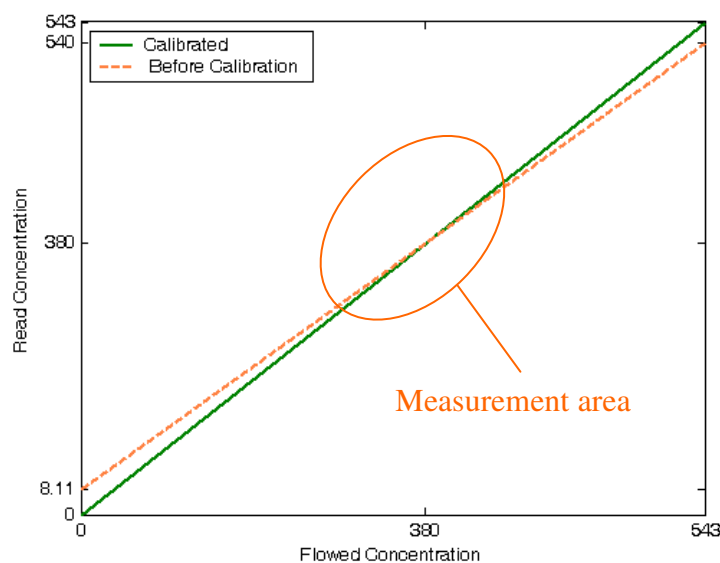


Figure 2.11: Calibration diagram for the LICOR. Concentrations are given in ppm

2.2.8 Soil moisture

Volumetric water content has been measured at 5 cm, 10 cm, 25 cm and 50 cm deep with CS615 water content reflectometers set horizontally. Two CS615 water content reflectometers have been installed vertically, one from 0 cm to 30 cm deep and a second from 30 cm to 60 cm deep. This type of sensor uses time domain reflectometry (TDR) methods that are based on the propagation characteristics of an electromagnetic wave on a transmission line. The probe consists of two 30 cm long stainless steel rods connected to a printed circuit board. High-speed electronic components on the circuit board are configured as a bistable multivibrator. The output of the multivibrator is connected to the probe rods, which act as a wave travel guide. The travel time of the signal on the probe rods depends on the dielectric permittivity of the material surrounding the rods and the dielectric permittivity depends on the water content. Therefore the oscillation frequency of the multivibrator is dependent on the water content of the media being measured. The CS615 output is essentially a square wave with amplitude of ± 0.7 volts with respect to the system ground. The period is then converted into volumetric water content thanks to a calibration equation.

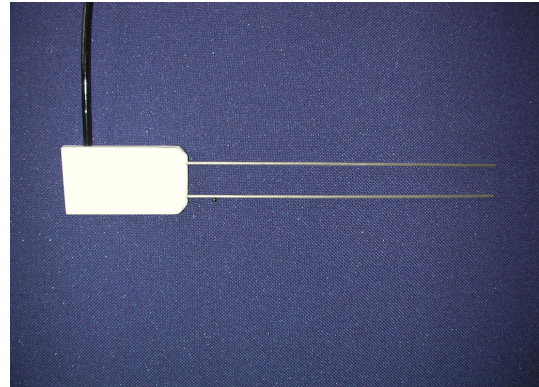


Figure 2.12: Soil moisture probe

2.2.9 Stream flow



Figure 2.13: V notch weir

In the small adjacent stream, about 10m from the tower, a Thalimedes device collects the height of water at the 90° V notch weir section. The catchment area at this point is 15 ha. Data are recorded at 15 minutes intervals, and then transformed into 30 minutes interval in order to be used with the meteorological measurements.

The associated formula to convert height (m) into flow (L/s) is:

$$Q = 1390 \times h^{2.5} \quad (2.13)$$

Chapter 3

Data analysis

Table of Content

3.1 General meteorological data.....	19
3.1.1 Global data	19
3.1.2 Precipitation and water balance.....	20
3.2 Momentum flux filter	21
3.3 CO ₂ Filter.....	23
3.3.1 Nighttime.....	23
3.3.2 Daytime	23
3.4 Gap filling function	23
3.4.1 Nighttime data.....	24
3.4.2 Daytime data	25
3.5 Six weeks gap filling	28
3.5.1 Site position method.....	28
3.5.2 Inverse Spring method	29
3.6 Corrections	30
3.6.1 Day length correction	30
3.6.2 Webb Correction.....	32
3.7 Final results and discussion.....	34
Site	39
References.....	40

3.1 General meteorological data

3.1.1 Global data

Daily air temperatures have a very small range of variation during the year, going from a maximum of 23° C to a minimum of 0° C, with an average value of 15° C. in summer and 5° C. in winter. No frost has been noticed during the study period (Figure 3.1.a). Surface temperatures show much bigger variations, seasonally and daily speaking (figure 3.1.a). As for the soil temperature at 5 cm deep, it follows the same annual pattern as air temperature, except for the night parts where the soil temperature does not cool as quickly as the air. The soil has a bigger inertia than the air.

The relative air humidity stays high throughout the year, and fluctuates a lot on the daily basis. However, spring distinguishes itself from the other seasons with drier peaks down to 40 % of relative humidity (Figure 3.1.c). Those points correspond to lows in the precipitation and soil moisture curves (Figure 3.1.b & d).

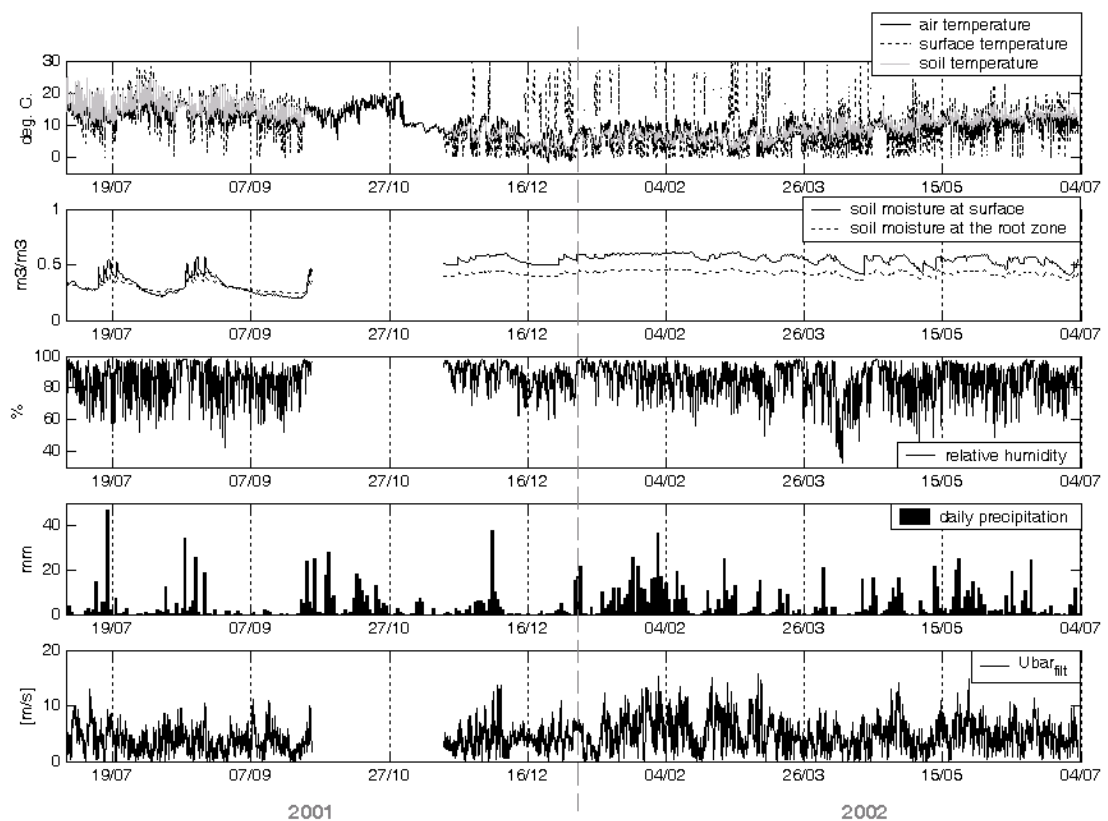


Figure 3.1: Global meteorological data. (a) :air , surface & soil temperatures, (b): soil moisture at 5 cm deep and at 20 cm deep, (c): relative humidity, (d): daily precipitation in mm, (e): Wind speed in m/s.

The soil moisture at 5 cm deep and at 20 cm deep follows the same pattern, with values around $0.35 \text{ m}^3/\text{m}^3$ for both in summer and $0.6 \text{ m}^3/\text{m}^3$ at 5cm and $0.5 \text{ m}^3/\text{m}^3$ at 20 cm in winter (Figure 3.1.b). The 20 cm deep curve is flatter than the other one; being deeper, the soil layer reacts in a slower way to each rain event. For each drier period, the curves come nearer, but there is clearly a different soil behaviour for the first part of the graph, where the soil moisture is almost the same at 5 cm deep and 20 cm deep (period before the gap which is summer 2001), and the second part, where there's about $0.1 \text{ m}^3/\text{m}^3$ of difference between the two depths (period after the gap which is winter 2001/2002 and spring 2002). This shift can be explained by the especially dry summer in 2001. The water then goes directly from one layer to another, whereas in winter, the surface layer is saturated and water percolates slowly from one layer to another.

Thirty minutes averages of wind direction were from the west 40 % of the time. The mean wind velocity at 10 m high is about 4.5 m/s with peaks in wintertime up to 15m/s (figure 3.1.e).

3.1.2 Precipitation and water balance

There is no clear seasonality in precipitations, as can be seen on Figure 3.1 d. Summer rains are more intermittent and intense but no dry season is observed. Rains are usually of small intensity with rainfalls below 0.1 mm per 30 minutes 85 % of the time (Figure 3.2). Figure 3.3 emphasizes that rains are likely to occur more in the morning, with a lower frequency after mid-afternoon. The cumulative amount of precipitation during the 12 months study (July 2001 to July 2002) period is 1600 mm (Figure 3.4), which is above the mean annual precipitation of 1400 mm (average over five years at this site).

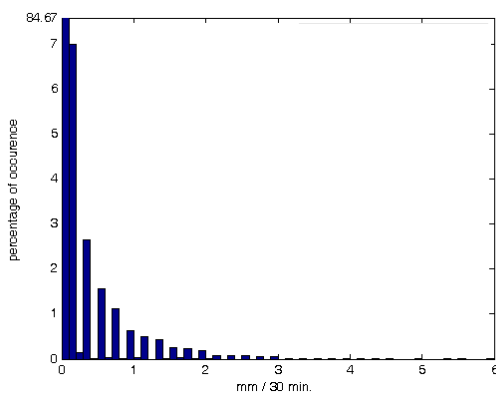


Figure 3.2: Amplitude of rain events.

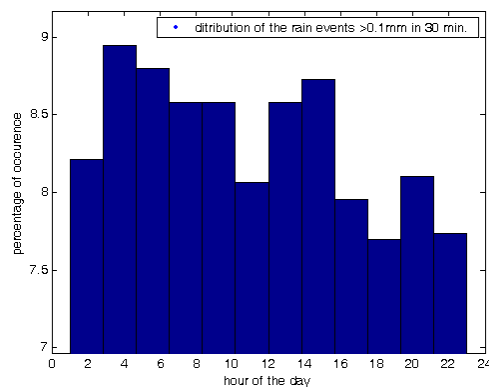


Figure 3.3: Distribution of the rain events in the day

The net radiation has an annual variation, with summer (30 minutes average) values ranging from $600 \text{ W}/\text{m}^2$ to $-80 \text{ W}/\text{m}^2$ and winter ranging from $200 \text{ W}/\text{m}^2$ to $-80 \text{ W}/\text{m}^2$. In the partitioning of the water balance, the biggest part of the radiation is used in latent heat flux which is pictured here in cumulative evaporation in mm throughout the year, in comparison with the cumulative precipitations and stream flow (Figure 3.4). In summer, almost all of the precipitation is evaporated with hardly anything arriving to the stream. A shift happens in late October when the stream flow

becomes the main receiver of precipitation via the runoff phenomenon. Evaporation shows a flat part when radiation is lower in winter.

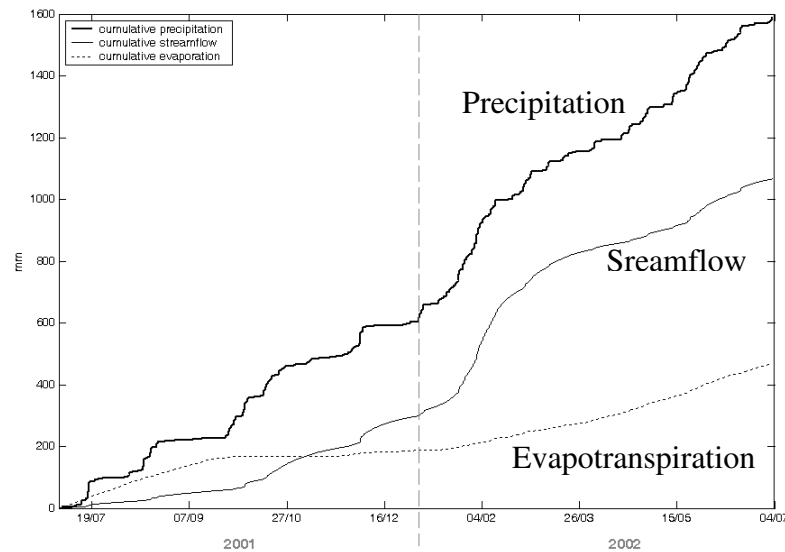


Figure 3.4: Rainfall water balance partition: cumulative precipitation is shared between cumulative stream flow and evaporation

3.2 Momentum flux filter

Carbon sequestration reflects the difference between two larger fluxes, respiratory efflux during the night and photosynthetic uptake during the day. A small underestimation of nocturnal flux can cause a large overestimation of long-term sequestration (Goulden et al., 1996; Baldocchi et al., 1996; Moncrieff et al., 1996; Schmid et al., 2000; Valentini et al., 2000). Numerous researchers suspect uncertainties in eddy diffusivity at night (Falge et al., 2001). The nocturnal period include conditions such as cold air drainage, sporadic mixing, and fluctuations in vertical wind too small to be resolved by the sonic anemometer. During a poorly mixed period, a reduction in the measured vertical flux of CO_2 is usually found (Goulden et al., 1996). In the literature, definitions of poor mixing use a condition on the momentum flux $u^* < u^*_{\text{critical}}$, with u^*_{critical} varying from 0.15 up to 0.4 m/s.

Figure 3.5 shows the behaviour of the mean CO_2 flux at night over the study period when terms corresponding to momentum fluxes below a varying u^*_{critical} have been removed. Tested u^*_{critical} are ranging from 0 to 1 m/s at 0.005 m/s intervals.

There is a shift for u^*_{critical} around 0.5 m/s. This value should be a good way to define poorly mixing, but it will induce a removal of 76.7% of the measurements made at night during the study period. Thus, the remaining values would not be representative enough of the period. That is why, a critical value of 0.3 m/s has been chosen (during a work session with G. Katul, September 2002) as a condition for bad nighttime mixing conditions for CO_2 flux measurements.

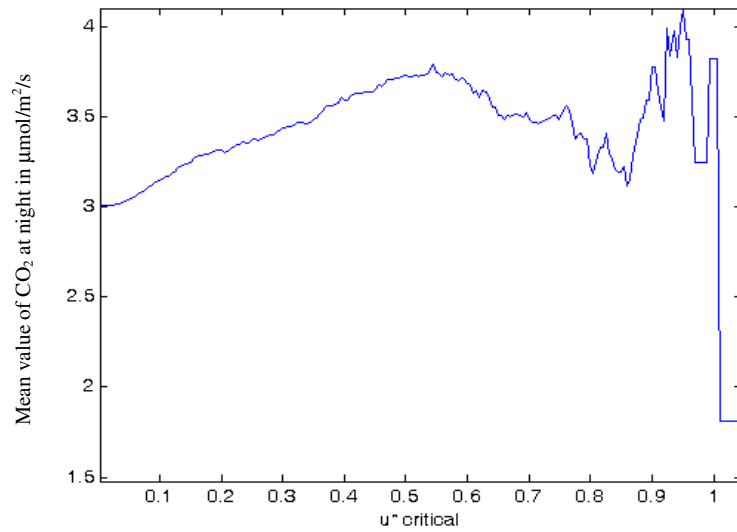


Figure 3.5: Behaviour of the mean CO_2 flux at night under varying u^* critical.

Figure 3.6 represents the momentum flux during the whole study period (day and night). The grey line marks the 0.3 m/s border under which data should be removed. It can be seen on the frequency histogram of the momentum flux that values below 0.3 m/s (which we described earlier as bad wind conditions for CO_2 measurements during the night) happen 45.5 % of nighttime. This value is consistent with the average data coverage during a year usually admitted for eddy covariance device, 65% only because of system failure or data rejection.

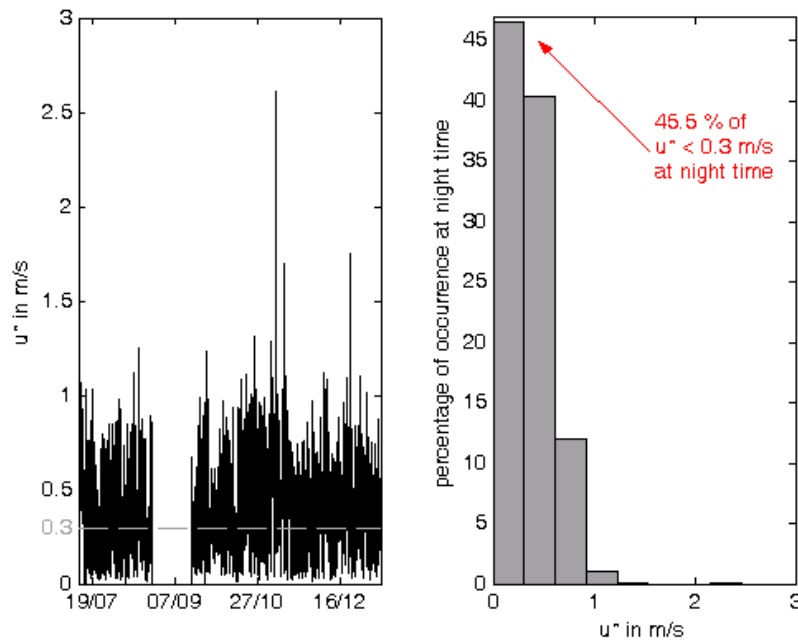


Figure 3.6: Momentum flux during the study period and its frequency histogram

3.3 CO₂ Filter

3.3.1 Nighttime

It has been seen on the later section, that CO₂ flux measurements are sensitive to the physical environment and that consequently data corresponding to low wind conditions at nighttime must be removed. Those are not the only measurements that should be filtered. Indeed, a respiration flux above 15 $\mu\text{mol}/\text{m}^2/\text{s}$ (the convention of flux is taken positive away from the surface) during the night cannot be seen on a grassland site. In the same way, photosynthesis cannot occur without any light. Thus negative flux should be filtered out at nighttimes. Moreover, some gaps in data already happened because of a power cut off during six weeks in autumn 2001 (October the 1st to November the 15th, 2001).

The conditions applied on CO₂ nighttime fluxes are summed up here.

$F_c = \emptyset$ when :

- $u^* < 0.3 \text{ m/s}$
- $F_c < 0 \mu\text{mol}/\text{m}^2/\text{s}$
- $F_c > 15 \mu\text{mol}/\text{m}^2/\text{s}$

3.3.2 Daytime

No physical environmental conditions are applied to filter CO₂ flux at day times. The only removed data are those with a photosynthetic flux below - 35 $\mu\text{mol}/\text{m}^2/\text{s}$.

The conditions applied on CO₂ day fluxes are summed up here.

$F_c = \emptyset$ when :

- $F_c < -35 \mu\text{mol}/\text{m}^2/\text{s}$

3.4 Gap filling function

Once CO₂ flux bad data have been removed in a satisfying way, some methods have to be found to fill the gaps, in order to be able to establish the carbon balance for different time scale: from daily budget to annual budget. Gap filling functions applied here are mostly non-linear regressions (Lai et al., 2002; Falge et al., 2001; Goulden et al., 1996). Those latter capture and preserve the response between fluxes and meteorological driving forces. To describe effects due to diurnal patterns, daytime and nighttime data were addressed separately.

3.4.1 Nighttime data

For nighttime data, the ecosystem respiration is known to be linked to the soil temperature (Lloyd & Taylor, 1994). The temperature used here is the soil temperature at 5 cm deep. The different functions tested are: a linear relationship, an exponential relationship, Arrhenius function and the so called Q_{10} relations firstly with 25 °C as reference, and then 10°C as reference.

The Matlab curve fitting toolbox has been used to determine parameterisation of those functions, as well as the goodness of each fitting in term of Sum of Squares Error (SSE), Root-Square (R^2), adjusted Root Square (adjusted- R^2), and Root Mean Squared Error (RMSE). For SSE and RMSE the closer to 0 the better, whereas for R^2 and adjusted- R^2 the closer to 1 the better.

	Equation	Coefficients	SSE	R^2	Ad. R^2	RMSE
Linear fitting	$F_{ni} = a \times t_{soil} + b$	a=0.164± 0.022 b=0.964± 0.223	6.21e4	0.0351	0.0349	3.27
Exp. fitting	$F_{ni} = a \times e^{(b \times t_{soil})}$	a=1.047± 0.122 b=0.0863± 9.6e-3	6.14e4	0.0457	0.0455	3.25
Arrhenius function	$F_{ni} = a \times e^{\left(\frac{b-c}{t_{soil}}\right)}$	a=2.744± 4.6e6 b=0.8836± 1.68e6 c=5.045± 0.473	5155	0.285	0.284	1.71
Q_{10} function with 25°C	$F_{ni} = a \times b^{\left(\frac{t_{soil}-25}{10}\right)}$	a=12.73± 0.99 b=2.34± 0.14	4639	0.356	0.356	1.62
Q_{10} function with 10°C	$F_{ni} = a \times b^{\left(\frac{t_{soil}-10}{10}\right)}$	a=3.558± 0.08 b=2.34± 0.14	4639	0.356	0.356	1.62

Table 3.1: Goodness of fit for nighttime functions

Table 3.1 gives coefficients for each function and its goodness of fit. The Q_{10} function with 10°C as a reference seems more appropriate in Ireland since soil temperatures hardly go over 20°C. The coefficient ‘a’ in the equation is then the ecosystem respiration when the soil temperature is at 10°C, $R_{10}=3.558 \mu\text{mol}/\text{m}^2/\text{s}$, which is easily checkable, and seems consistent with other measurements (Lai et al., 2002).

Figure 3.7 shows that the regression of nighttime CO_2 fluxes against soil temperature is a very scattered plot. This is likely linked to the different respiration sources, leaf and soil. They have not been separated in this study but their contribution changes over time and in response to different developmental factors. However, this separation is not possible without independent measurements. Figure 3.7 pictures the three best fits for nighttime data which are the linear fitting, Q_{10} function and Arrhenius equation.

On view of those results, the Q_{10} function with 10°C has been selected for its good performances and therefore has been used to fill all the filtered data at nighttime.

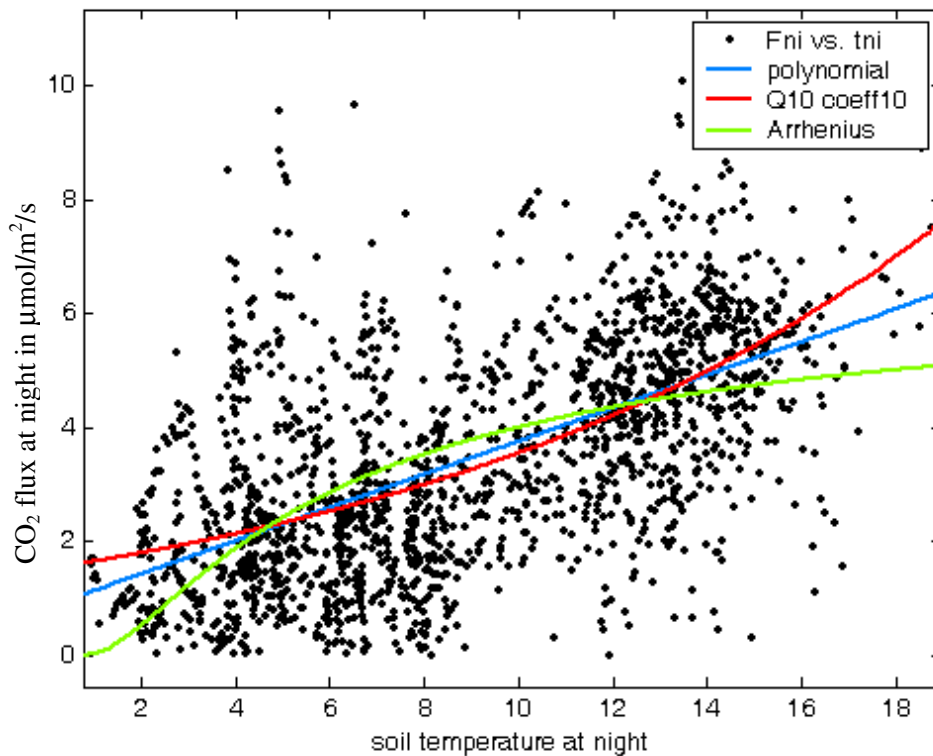


Figure 3.7: Three best fits for nighttime

3.4.2 Daytime data

In the same way, the net ecosystem exchange of CO_2 at daytime is known to be linked to the photosynthetic photon flux density Q in μmol of quantum/ m^2/s (Smith, 1938; Michaelis & Menten, 1913; Misterlich, 1991). The photosynthetic flux is obtained either by converting, with some approximations, 45 % of the incoming solar radiation from W/m^2 into μmol of quantum/ m^2/s or thanks to the PAR Lite instrument as explained in chapter 2.

The different functions tested are: a linear relationship, Smith formula, Michaelis-Menten (referred elsewhere to a rectangular hyperbola), Misterlich formula (Falge *et al.*, 2001), and Ruimy formula (Lai *et al.*, 2002; Ruimy *et al.*, 1995).

The Matlab curve fitting toolbox has been used, here as well, to determine parameterisation of those functions, and goodness of each fitting function. In the case of Mysterlich, Michaelis and Smith formula, the non-linear problem could only be resolved by holding some parameters constant. Indeed, the complete equations use the gross primary productivity at ‘optimum’ light $F_{GPP,opt}$, which is a function of the air temperature.

$$F_{GPP,opt} = \frac{F_{GPP,Tref} \times e^{\frac{(\Delta H_a \times (T_K - T_{ref}))}{(R \times T_K \times T_{ref})}}}{1 + e^{\frac{((\Delta S \times T_K - \Delta H_d))}{(R \times T_K)}}} \times \left(1 + e^{\frac{((\Delta S \times T_{ref} - \Delta H_d))}{(R \times T_{ref})}}\right) \quad (3.1)$$

With T_K the air temperature (in K), R the gas constant (8.314 J/K/mol), ΔH_a the activation energy in J/mol, ΔH_d the energy of deactivation (set to 215,000 J/mol), ΔS an entropy term (set to 730 J/K/mol) and $F_{GPP,ref}$ the carbon uptake at optimum light and reference temperature T_{ref} (298.16 K).

Matlab curve fitting toolbox cannot consider this kind of added variable data in a curve fitting study. However this variable does not fluctuate a lot, and has therefore been considered as a constant ‘b’ for Michaelis and Smith function in Table 3.2 that was set by curve fitting, and replaced by its mean (-24 $\mu\text{mol CO}_2 / \text{m}^2/\text{s}$) for Mysterlich function. In those three equations, ‘a’ corresponds to α , the ecosystem quantum yield and ‘c’ is the daily respiration.

	Equation	Coefficients	SSE	R ²	Ad. R ²	RMSE
Linear fitting	$F_d = a \times Q + b$	a = -22.71 ± 0.62 b = 22.68 ± 7	2.51e7	0.694	0.694	105.4
Michaelis function	$F_d = \frac{a \times Q}{\left(1 - \frac{Q}{2000} + \frac{a \times Q}{b}\right)} + c$	a = -4.555 ± 0.32 b = -6.467 ± 0.171 c = 0.663 ± 1.41	2.15e5	0.0175	0.0173	6.33
Smith function	$F_d = \frac{a \times b \times Q}{\sqrt{b^2 + (a \times Q)^2}} + c$	a = 0.0217 ± 1.2e-3 b = -17.51 ± 0.57 c = 1.51 ± 0.262	8.83e4	0.596	0.596	4.06
Mysterlich function	$F_d = -24 \times \left(1 - e^{\left(\frac{a \times Q}{-24}\right)}\right) + c$	a = 0.019 ± 7.2e-4 c = 0.93 ± 0.23	9.1e4	0.584	0.579	4.12
Ruimy function	$F_d = \frac{a \times Q \times b}{(a \times Q + b)} + c$	a = 0.03163 ± 0.127 b = -24.86 ± 1.07 c = 2.037 ± 0.31	8.82e4	0.597	0.597	4.06

Table 3.2: Goodness of fit for daytime functions

The goodness coefficients given in table 3.2 underline the better performances for the Smith's, Misterlich's and Ruimy's formulations than for the others presented here. As for Ruimy's equation, the coefficient found here correspond to:

- α_p = mean apparent quantum yield = 0.0316
- F_{sat} = CO₂ flux at light saturation = -24.86 $\mu\text{mol}/\text{m}^2/\text{s}$
- R_0 = mean net CO₂ flux during light absence = 2.037 $\mu\text{mol}/\text{m}^2/\text{s}$

For two pine forest sites, Lai *et al.* give similar values: α_p are 0.029 and 0.044, F_{sat} are -26 and -31 $\mu\text{mol}/\text{m}^2/\text{s}$, R_0 are 3.9 and 4.6 $\mu\text{mol}/\text{m}^2/\text{s}$. Considering that the types of site are very different and explain for smaller values, in our case, for the CO₂ flux at light saturation and light absence, those results support the reliability of the coefficients found with Matlab curve fitting toolbox for our study.

Figure 3.8 pictures the three best fit for daytime data, Misterlich's, Smith's and Ruimy's fits. The CO₂ flux plot against the photosynthetic photon flux is much less scattered than for the nighttime data. The main trend is easily noticeable. Thus trusting either the fitting coefficients or the visual aspect of the fits, Ruimy's formulation shows best results. This later has been used to fill all missing or filtered data at daytime.

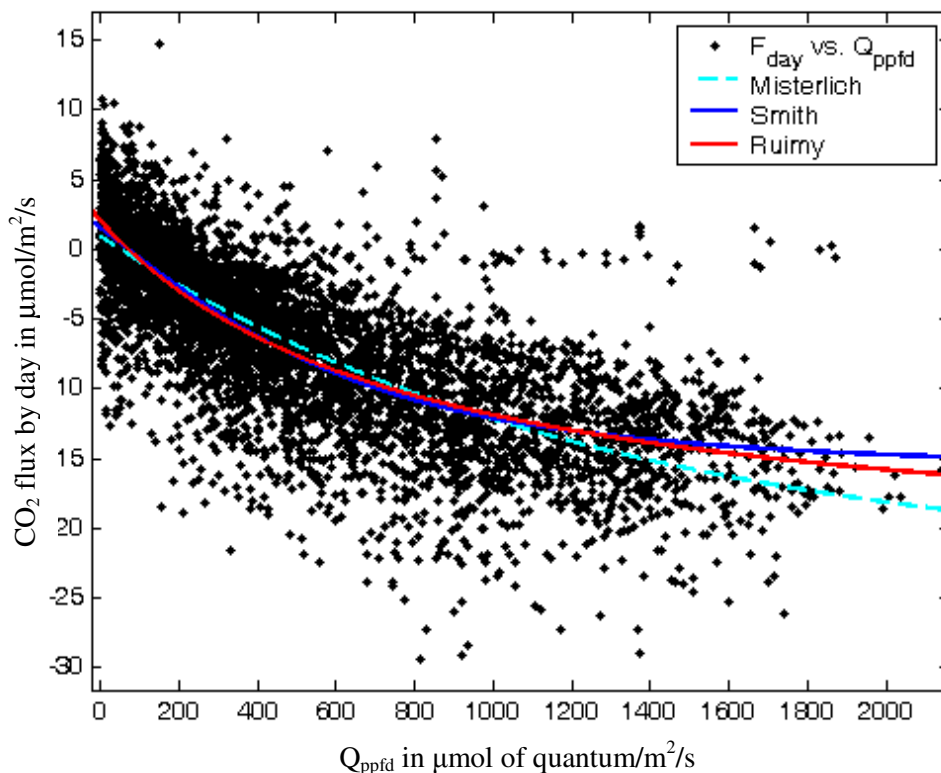


Figure 3.8: Three best fits for daytime

3.5 Six weeks gap filling

The equations that have been chosen to fill daytime and nighttime gaps can be used for short time period such as 1hr or 2hr, and for long time gaps of the order of a month or more (Lai et al., 2002; Falge et al., 2001). Indeed, we had sufficient data over the study period to consider that the coefficients found in the previous section can be used as an efficient modelling scheme even for a long period. However those equations still need some data inputs: soil temperature at 5 cm deep for Q_{10} function and the photosynthetic photon flux for Ruimy's formula.

As for the soil temperatures, the gap in inputs has been filled thanks to data collected by a nearby weather station. Thus nighttime CO_2 fluxes between the days of year 272 and 319 have been directly provided by Q_{10} function as for rejected data.

At that stage of the study period, the PAR Lite sensor was not installed yet, and as it has been seen in the introduction part, incoming radiation have not been recorded during the days of year 272 and 319. Two methods have been examined to obtain a continuous photosynthetic photon flux.

3.5.1 Site position method

An estimation of the direct and diffuse short-wave irradiance can be found thanks to the location of the sun in the sky (Campbell & Norman, Environmental Biophysics). This later is described in terms of zenith angle (ψ , the angle measured from the vertical) and its azimuth angle (AZ, angle from true north measured in horizontal plane). With the exact coordinates of the site (52° North latitude ϕ , 8° 30' W longitude χ), and the calendar day in Julian day (J), the time of solar noon (t_0) and the solar declination equation can be found.

The time of solar noon is calculated from:

$$t_0 = 12 - \chi_{co} - \Theta \quad (3.2)$$

where χ_{co} is the longitude correction (+ 1/15 hour for each degree east of the nearest standard meridian, in this case + 6.5/15 from the 15° meridian), and Θ is the equation of time (15 or 20 minute correction which depends on calendar day).

$$\Theta = \frac{-104.7 \sin(f) + 596.2 \sin(2f) + 4.3 \sin(3f) - 12.7 \sin(4f) - 429.3 \cos(f) - 2 \cos(2f) + 19.3 \cos(3f)}{3600} \quad (3.3)$$

where,

$$f = 279.575 + 0.9856 \times J \quad (3.4)$$

Then the zenith angle is calculated from:

$$\cos \psi = \sin \phi \times \sin \delta + \cos \phi \times \cos \delta \times \cos(15 \times (t - t_0)) \quad (3.5)$$

where ϕ is the latitude, t is time, t_0 is the time solar noon and δ is the solar declination given by

$$\sin \delta = 0.39785 \times \sin(278.97 + 0.9856 \times J + 1.9165 \times \sin(356.6 + 0.9856 \times J)) \quad (3.6)$$

Computation of the short wave component of the radiant energy budget of an organism requires estimates of flux densities for at least three radiation streams: direct irradiance on a surface perpendicular to the beam S_p , diffuse sky irradiance on a horizontal plane S_d and reflected radiation from the ground S_r . The total irradiance is then written:

$$S_t = S_p \times \cos \psi + S_d \quad (3.7)$$

Clear sky S_p is:

$$S_p = S_{po} \times \tau^m \quad (3.8)$$

where S_{po} is the extraterrestrial flux density in the short waves waveband, normal to the solar beam. τ is the atmospheric transmittance and m is the optical air mass number, or the ratio of slant path length through the atmosphere to zenith path length. For zenith angles less than 80° , refraction effects in the atmosphere are negligible, and m is given by:

$$m = \frac{P_a}{101.3 \times \cos \psi} \quad (3.9)$$

where p_a is the atmospheric pressure at the observation site.

Of the sun radiation that enters the atmosphere, part reaches the ground as beam radiation, part is absorbed by the atmosphere, part is scattered back to space, and part is scattered downward toward the ground. The down-scattered part is called sky diffuse radiation. Approximate values can be computed for sky diffuse radiation on clear days using an empirical equation:

$$S_d = 0.3 \times (1 - \tau^m) \times S_{po} \times \cos \psi \quad (3.10)$$

Then, we obtained the photosynthetic photon flux from equation (2.5).

Figure 3.9 (c) shows in green the photosynthetic photon flux thus obtained for the gap period. It is obvious that this flux is too small, and cannot be used to fill the gap in our data. The reason why the equations cited above do not work in this case, is that they refer to clear days only. No simple model describes the impact of clouds. But, the climate in Ireland is such that we cannot overlook the clouds effects.

3.5.2 Inverse Spring method

The second method used is more empirical. Because of the earth movement, the solar position fluctuates during the year and the amount of radiation received by a given point increases during spring and decreases during autumn. We assumed here that the rates of increase and decrease were similar enough to use one for another. The original graph for the photosynthetic photon flux Q_{PAR} (Figure 3.9 a) has a gap from October the 28th to November the 15th. We inverted it in order to have July 2002 on

the left and July 2001 on the right (Figure 3.9 b). In doing so spring 2002 can be used to fill the gap in autumn 2001. We took the best fitting part of (b), and injected it in (a). Thus figure 3.9 c was obtained and pictures a continuous photosynthetic photon flux during the whole study period. The red part shows the filled portion.

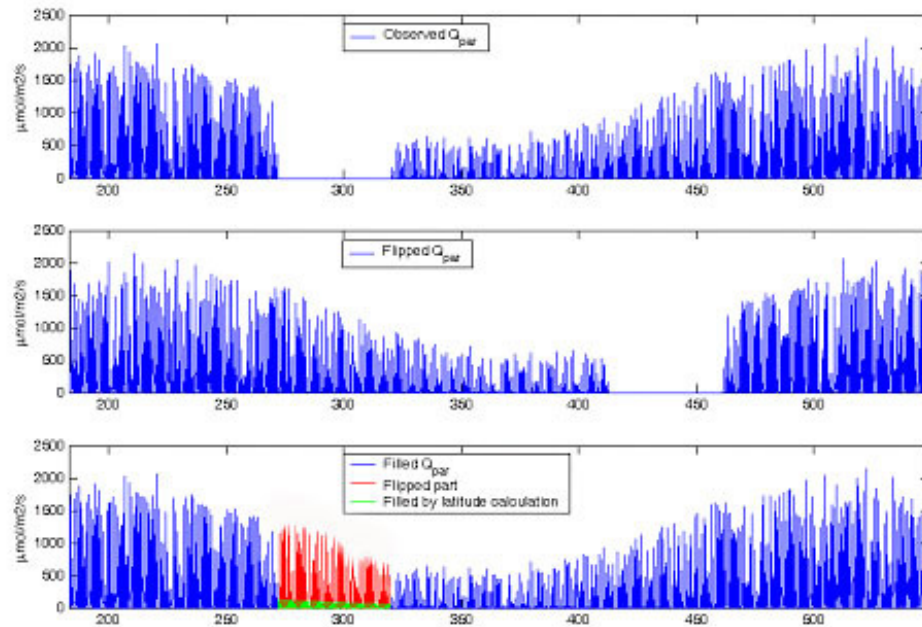


Figure 3.9: Inverse spring Q_{par} method. (a) is the measured Q_{par} curve with the six week gap, (b) is the inverted Q_{par} curve with July 2002 on the left of the graph and July 2001 on the right, (c) shows the measured Q_{par} in blue with the part from the inverted graph(b) in red and in green the Q_{par} from the site position method.

3.6 Corrections

3.6.1 Day length correction

At that point, we had a complete set of data over the study period. However, when the time came to draw the cumulative uptake of CO_2 or C in T/ha/y, we ended with very high values for a grassland site: almost 24 T of CO_2 /ha/y or 6.5 T of C/ha/y (Figure 3.10 dark blue curve). The filters, applied to CO_2 flux measurements, all distinguish daytime and nighttime values. The question underneath is then how to have a good definition of night or day length. Figure 3.10 shows the cumulative uptake of C or CO_2 for the site during the year of study with different definitions for day length. The two first used were based on a fixed night between two decimal hours:

- 0.85/0.2 which is a night from 20 H 30 to 5 H all the time (in blue)
- 0.7/0.35 which is a night from 17 H to 8H30 all the time (in red)

Those two definitions are the most extremes and do not fit the reality since the night length is the same in summer and in winter. However, it emphasizes the huge impact of night length definition, since with an uptake of only 1.75 T of CO₂/ha/y the second formulation induced a change of 70 % in our previous results. The longer the night, the greater the part of respiration in the carbon budget and the smaller the cumulative uptake.

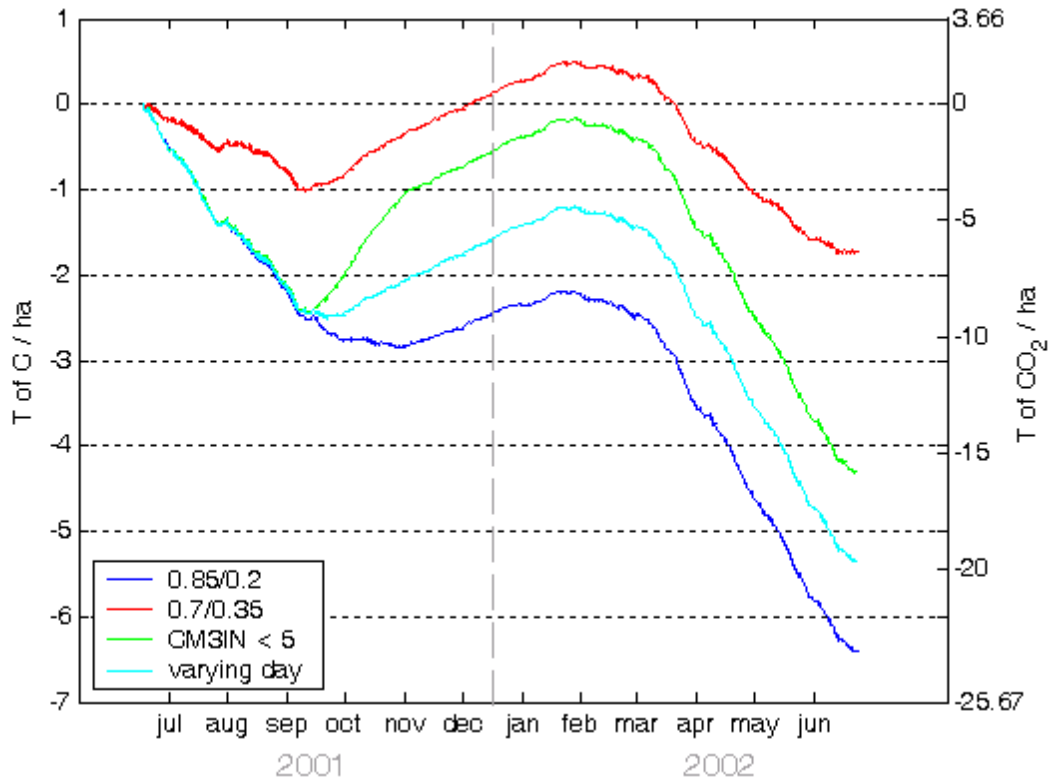


Figure 3.10: CO₂ and C cumulative uptake in T/ha/y according to four different expressions of day length in bad data filters.

The two other tested formulations of night duration allow for the seasonality of day length. The first (Figure 3.10 in green) is based on the amount of incoming solar radiation. Night begins when those radiation are below a very small value such as 5 W/m² (against 950 W/m² at noon in summer). The second (Figure 3.10 in cyan) is an astronomical definition where sunrise and sunset correspond to a zenith angle of 90°. The half daylength, which is the time (in degrees) from sunrise to solar noon, can be expressed as:

$$h_s = \cos^{-1} \left(\frac{\cos \psi - \sin \phi \times \sin \delta}{\cos \phi \times \cos \delta} \right) \quad (3.11)$$

where $\cos \psi$ is null for the geometrical sunrise and sunset, ϕ is the latitude and δ is the solar declination.

The time of sunrise (t_r) and sunset (t_s) are then:

$$t_r = t_o - \frac{h_s}{15} \quad (3.12)$$

$$t_s = t_o + \frac{h_s}{15} \quad (3.13)$$

The two resulting curves stand between the former expressions. It can be noticed that the first and last third of those follow the short night expression (Figure 3.10 in blue) whereas the second one follows the slope of the long night expression (Figure 3.10 in red) so that night in Ireland fluctuates approximately between 8.30 pm and 5 am in summertime, and 17 pm and 8.30 am in wintertime. The radiation expression curve (Figure 3.10 in green) shows a strange behaviour during the six weeks filled gap with a very strong respiration slope. That's why we kept the astronomical definition of night as the best one. This is the one that has been used for the rest of the study.

3.6.2 Webb Correction

When the turbulent flux of any constituent is measured by eddy covariance, account may need to be taken of the simultaneous flux of any entity, in particular heat or water vapor, which causes expansion of the air and thus affects the constituent's density (Webb *et al.*, 1980). The eddy correlation method described in Chapter 2 uses some close approximations to end up with the simple equation (2.11). For the CO₂ flux, we have:

$$F_c \cong -\overline{w' \rho_c'} \quad (2.11)$$

However, the full equation should be written

$$F_c = -\overline{w' \rho_c'} - \overline{w} \times \overline{\rho_c} \quad (3.14)$$

where the average wind velocity should be replaced by

$$\overline{w} = \frac{\overline{w' \rho_v'}}{m_v} \times \frac{R \times T}{(p - e)} + \frac{p}{(p - e)} \times \frac{\overline{w' T'}}{T} \quad (3.15)$$

where p is the atmospheric pressure (in mb), e the vapor pressure (in mb), the air temperature (in Kelvin), m_v and ρ_v the molecular weight and density of water vapor constituent, w' the instantaneous wind velocity and R the gas constant.

So that the 'Webb' corrected expression of the CO₂ flux is:

$$F_c = -\overline{w' \rho_c'} - \frac{R \times T \times \overline{\rho_c}}{m_v \times (p - e)} \times \overline{w' \rho_v'} - \frac{p \times \overline{w' T'} \times \overline{\rho_c}}{T \times (p - e)} \quad (3.16)$$

In CO₂ flux measurements, the magnitude of the correction will commonly exceed that of the flux itself (Webb *et al.*, 1980).

In our case, the 'Webb' correction has been applied to the CO₂ flux with the astronomical definition of the night length. The cumulative uptakes of carbon during the study period, with and without this correction are respectively 3.8 T of C/ha/y and 5.3 T of C/ha/y (Figure 3.11). So that the changes induced by the Webb correction represents 28 % of the previous value.

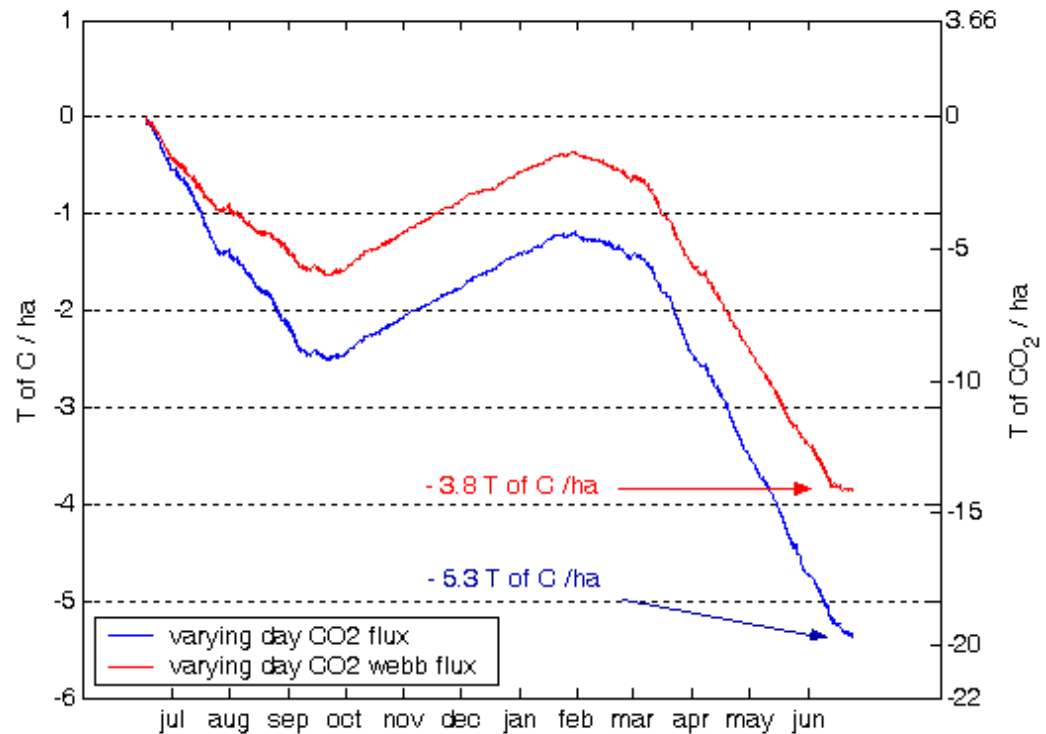


Figure 3.11: Cumulative uptakes of C and CO₂ in T/ha/y with the Webb correction (in red) and without it (in blue)

Figure 3.12 pictures the CO₂ fluxes per month with the Webb correction (in red) and without it (in blue). It emphasizes the impact of the correction at each month of the year, so that it can be seen that the Webb correction reduces both the respiration and the photosynthetic components. The flux ends with a smaller uptake as a sink of carbon from July to September 2001 and from February to June 2002 with a difference up to 100 g of CO₂ /m²/month, as well as a smaller release as a source of carbon in December with 20 g of CO₂ /m²/month of difference.

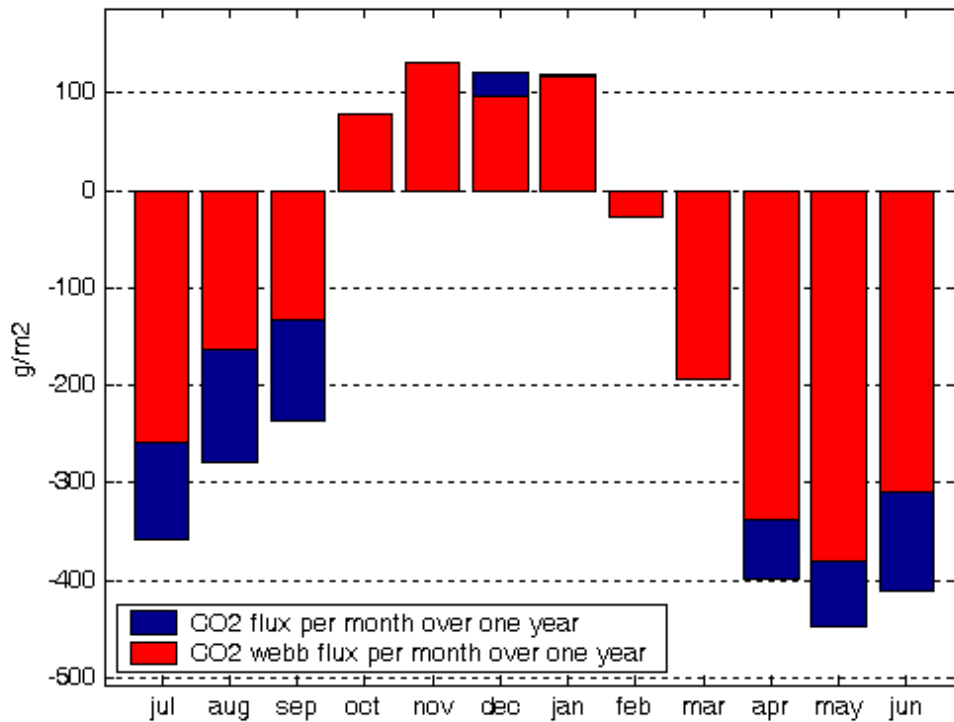


Figure 3.12: CO₂ fluxes per month in g/m² with the Webb correction (in red) and without it (in blue).

3.7 Final results and discussion

Two extreme days from the middle of the study period were selected to show the typical 30 minutes averaged CO₂ fluxes throughout a winter and a spring day (Figure 3.13). *In all figures, the photosynthesis flux is taken negatively, so that an uptake of carbon by the site is a negative value. The comparison fluxes from other sources have been converted to this sign convention.* The spring day curve (March the 23rd) corresponds to the highest flux of the study period with a maximum of -1.2 mg of CO₂ /m²/s at midday and a nighttime flux of 0.15 mg of CO₂ /m²/s. This day was clear and the photosynthesis process lasted from about 5 am to 8.30 pm, that is a 15.5 hours daylength. On the contrary, the winter day curve (January the 8th), is the smallest day flux of the study period with a maximum of -0.08 mg of CO₂ /m²/s only at midday and a nighttime flux of 0.12 mg of CO₂ /m²/s. The photosynthesis process lasted from about 8.30 am to 5 pm, that is an 8.5 hours daylength. This graph shows well the link between daylength and photosynthesis process, as well as the seasonal pattern for the CO₂ flux magnitude. The difference in the day part of the curves is much more important than the one for the nighttime so that the carbon budget for the 23rd of March is a net uptake whereas the 8th of January corresponds to a global loss.

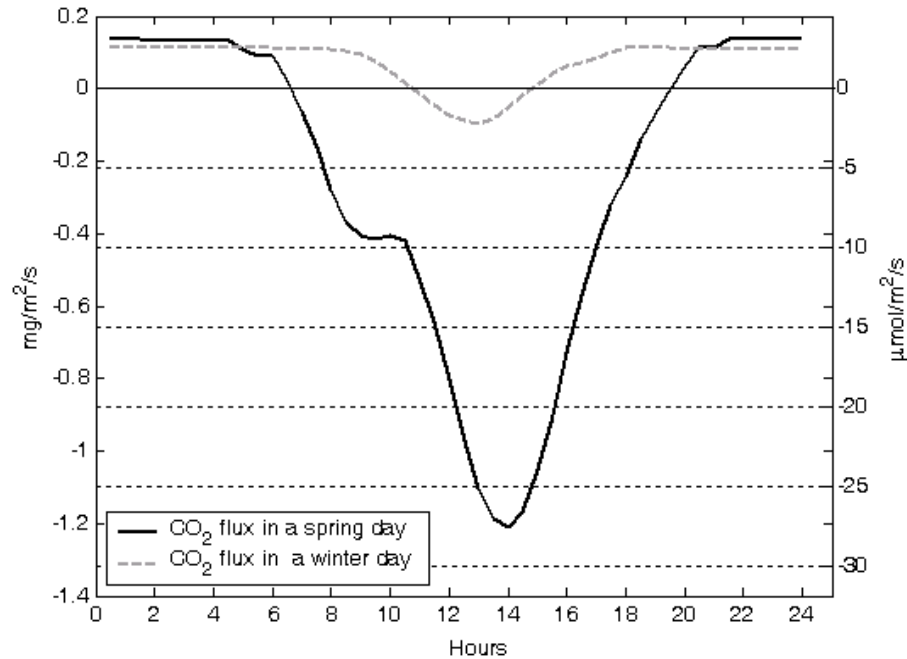


Figure 3.13: Maximum and minimum day pattern for CO₂ flux

However, those kinds of extreme events do not last for many consecutive days. Let F_{30} be the 30 minutes averaged CO₂ fluxes, $F_{d_{max}}$ the daily maximum of F_{30} . Then, the mean of $F_{d_{max}}$ over 20 consecutive days seems a more relevant indication for the seasonal fluctuation in magnitude, and a more reliable data to compare. For a spring period between the 21st of March and the 9th of April, averaged $F_{d_{max}}$ is -0.78 mg of CO₂ /m²/s, whereas for a winter period between the 14th of December and the 4th of January, averaged $F_{d_{max}}$ is -0.145 mg of CO₂ /m²/s. These values are really consistent with those given by Frank & Dugas(2001) for a mixed-grass prairie at Mandan, ND, and Sims *et al.* (2001) for a southern plains prairie, at Woodward, OK (see Table 3.3 for a summary of results). The mean $F_{d_{max}}$ values for those site over 20 days period in summer and winter are respectively: -0.4 mg of CO₂ /m²/s (Mandan), -0.7 mg of CO₂ /m²/s (Woodward) in early July and -0.18 mg of CO₂ /m²/s (Mandan), -0.2 mg of CO₂ /m²/s (Woodward) in mid-September.

Figure 3.14 shows the daily uptake of CO₂ and the daily maximum temperature. The maximum daily uptake is in late March and reaches a value of -22 g of CO₂/m²/d, whereas the maximum daily release in winter is 12 g of CO₂/m²/d. Those values are consistent with data hold up in example in table 3.3 (Frank & Dugas, 2001;Dugas *et al.*, 1999; Sims & Bradford, 2001; Saigusa *et al.*, 1998). The sites of Mandan and Woodward give very similar values to our Irish case, while results from Temple and Japan are 1.36 and 1.8 times our for the uptake (-30 g of CO₂/m²/d and -40 g of CO₂/m²/d respectively). This can be explained by the very high leaf area index (LAI) for those sites in summer (3 and 4 against 2.5 for Dripsey). Moreover Mandan, which has the smallest value of uptake, has a very small LAI of 0.5 in summertime.

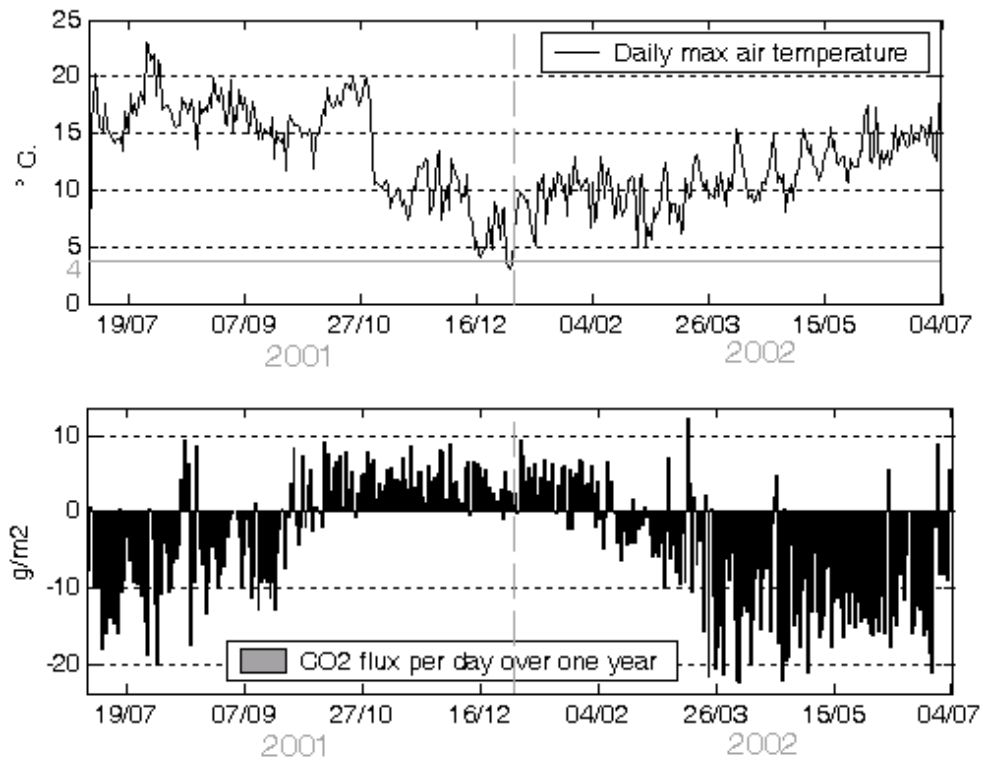


Figure 3.14: (a): Daily maximum temperatures, (b): daily CO₂ flux

Examining the monthly uptake of CO₂ shown in figure 3.15, the seasonal trend is clear. The part of the year for which the site behaves as a sink of carbon are from July to September 2001 and from February to June for 2002, while it behaves as a source of CO₂ from October 2001 to January 2002. If we convert those data in average daily uptake during a month, we obtain for May, which is the biggest month as a sink, -12.9 g of CO₂/m²/d and for November, which is the biggest month as a source 4 g of CO₂/m²/d. For the Woodward site (Sims & Bradford, 2001), the average for June, the biggest month as a sink, is only -6.4 g of CO₂/m²/s, and for March, the biggest month as a source, 1.5 g of CO₂/m²/s. Thus, although those two sites have very similar maximum and minimum daily CO₂ uptakes and fluxes, on a bigger scale (like an average on a month) discrepancies appear. It can be noticed, that the timing of the maximum and minimum uptake is also different for the two sites.

The divergence in results is even more obvious for the annual time scale, with a global uptake of -14 T of CO₂ /ha/y for Dripsey (Figure 3.16), whereas this later ranges between -3 and -3.45 T of CO₂ /ha/y for Mandan, Woodward and Temple sites (Table 2.3; Frank & Dugas, 2001; Dugas *et al.*, 1999; Sims & Bradford, 2001).

Figure 2.16 shows three almost linear parts:

- uptake of -6.74 g of CO₂ /m²/d for three months (Jul., Aug., Sept.)
- release of 3.2 for four months and a half (Oct., Nov., Dec., Jan.)
- uptake of -11.5 g/m²/d for three month and a half (Feb., Mar., Apr., Jun.)

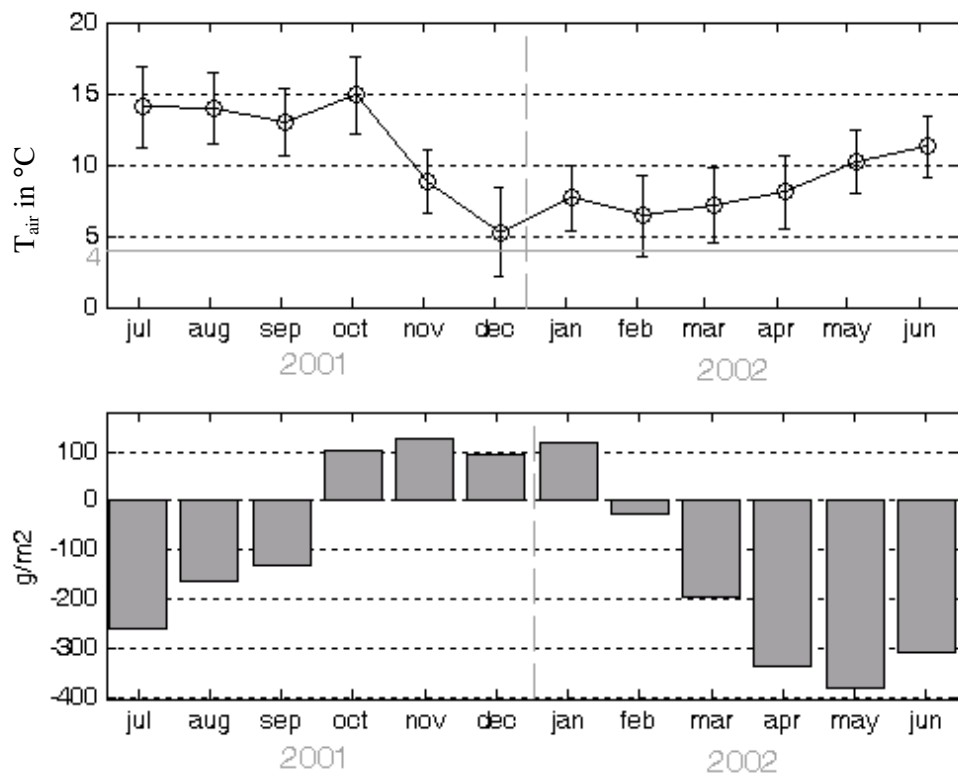


Figure 3.15: (a): mean & standard deviation for monthly air temperatures (b): Monthly CO_2 flux in g/m^2

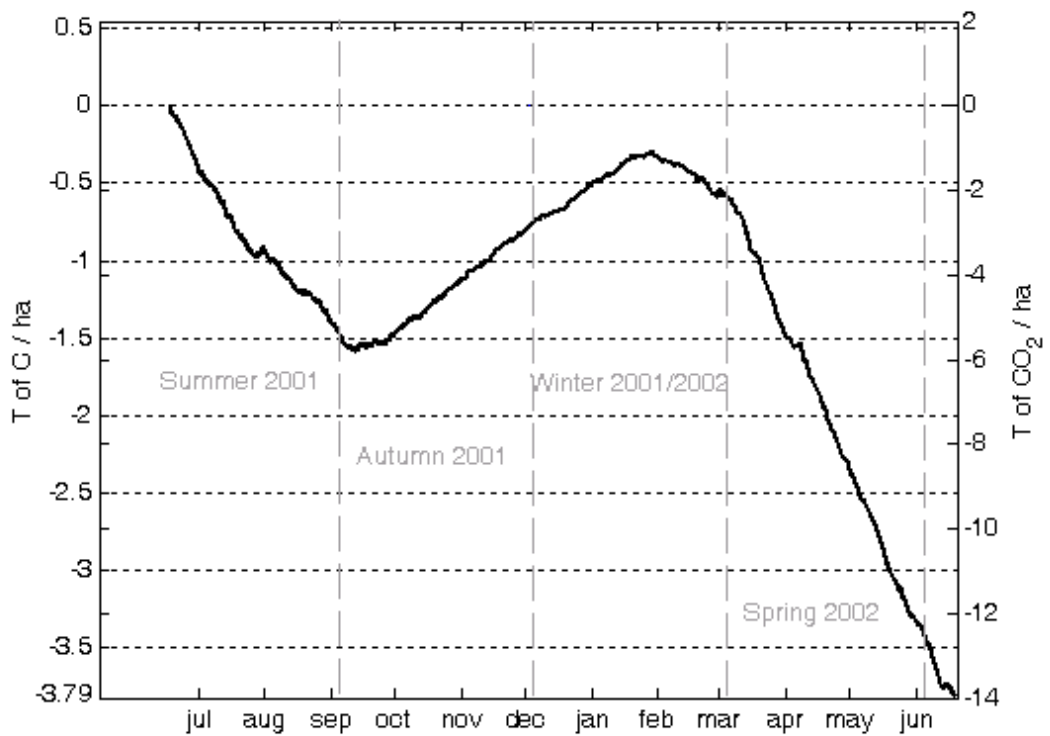


Figure 3.16: Cumulative uptake of C and CO_2 in T/ha

Several aspects can account for such a difference between Dripsey site and the others presented here. First, all of those sites have a different rainfall regime, going from low precipitations (404 mm /y for Mandan), medium precipitations (661 mm for Woodward and 880 mm for Temple) to high precipitations (1300 mm for central Japan and 1600 mm for Dripsey). It has been shown (Frank & Dugas, 2001), that short-term droughts during the growing season reduce CO₂ fluxes to near zero. Also, the timing and magnitude of precipitation events influence the total growing season flux and induce a considerable day-to-day variability in CO₂ fluxes (Figure 3.14). Moreover, the climate being very temperate in Ireland, very few days are under 4°C, which is a critical temperature for the photosynthetic process and no snow occurred in Ireland during the study period. Therefore, the leaf area index stays higher with a minimum value around 1 against 0 for the other sites (see table 3.3) and the sink period is extended from 4 months (Woodward, Temple) to 8 months (central Japan, Dripsey).

Another set of explanations can be found in the land use management. Indeed, neither Mandan site, nor Woodward or Temple sites have been fertilized, grazed or burned lately. However, Svecjar and Browning (1988) found a positive effect of fire on CO₂ flux in an Oklahoma tall grass prairie. As for Dripsey site, it has been seen in chapter 2 that the two cuts of silage during the study period may have affected the LAI and thus CO₂ flux at the beginning and also at the end of the study. The site was intensively grazed and Nitrogen fertilized. This later is likely to have increased the plant growth and the annual cumulative uptake.

Site	Mixed-grass prairie at Mandan, ND	Southern plains prairie, Woodward, OK	Native prairie at the Blackland research center, Temple, TX	A grassland site in central Japan	Grassland site in South West of Ireland
Authors	Frank, A.B., Dugas, W.A.	Sims, P.L., Bradford, J.A.	Dugas, W.A., Heuer, M.L, Mayeux, H.S.	Saigusa, N., Oikawa, T., Liu, S.	
Annual precipitation	404 mm	661 mm	880 mm	1300 mm	1600 mm
Latitude / Longitude	46°46' N 100°55' W	36°36' N 99°35' W	31°06' N 97°20' W	36° N 140° E	52° N 8°30' W
Grass category	C3 & C4 grasses mixed	C3 & C4 grasses mixed	C4 grass	C3 & C4 grasses mixed	C3 grass
Air Temperature range	< 0 in winter			14°C annual mean	From 0°C to 25°C 5°C mean in winter 15°C mean in summer
Leaf area index range	0 → 0.5		0 → 3	0.1 → 4	0.9 → 2.5 (estimate)
Mean of Fd_{max} over 20 days	-0.4 mg/m ² /s summer -0.18 mg/m ² /s winter	-0.7 mg/m ² /s summer -0.2 mg/m ² /s winter			-0.78 mg/m ² /s summer -0.145 mg/m ² /s winter
Daily CO₂ flux	Max -18 g/m ² /d Min 8 g/m ² /d	-20 g/m ² /d 15 g/m ² /d	-30 g/m ² /d 20 g/m ² /d	-40 g/m ² /d	-22 g/m ² /d 12 g/m ² /d
Annual uptake	3.45 T of CO ₂ /ha	3.2 T of CO ₂ /ha	3 T of CO ₂ /ha		14 T of CO ₂ /ha
Duration as a sink	6 months	4 months	4 months	8 months	8 months

Table 3.3: Summary of results for grasslands under different climates

References

- Baldocchi, D.D., Valentini, R., Running, S.R., Oechel, W., Dahlman, R., 1996. Strategies for measuring and modeling carbon dioxide and water fluxes over terrestrial ecosystems. *Global Change Biol.* 2, 159-168.
- Campbell, G.S., Norman, J.M. An introduction to environmental biophysics. Second Edition
- Dagnelie, P., 1991. *Théorie et Méthodes Statistiques*, Vol. 1. Presses Agronomiques de Gembloux, Gembloux, Belgium.
- Dugas, W.A., Heuer, M.L., Mayeux, H.S., 1999. Carbon dioxide fluxes over a Bermuda grass, native prairie, and sorghum. *Agric. For. Meteorol.* 93, 121-139.
- Falge, E., Baldocchi, D.D., Olson, R., et al., 2001. Gap filling strategies for defensible annual sums of net ecosystem exchange. *Agric. For. Meteorol.* 107, 43-69.
- Frank, A.B., Dugas, W.A., 2001. CO₂ fluxes over a northern semiarid mixed grass prairie. *Agric. For. Meteorol.* 108, 317-326.
- Goulden, M.L., Munger, J.W., Fan, S.M., Daube, B.C., Wofsy, S.C., 1996. Measurements of carbon sequestration by long-term eddy covariance: methods and critical evaluation of accuracy. *Global Change Biol.* 2, 169-182.
- Lai, C.-T., Katul, G., Butnor, J., Ellsworth, D., Oren, R., 2002. Modelling night-time ecosystem respiration by a constrained source optimization method. *Global Change Biology*, 8, 124-141.
- Lloyd, J., Taylor, J.A., 1994. On the temperature dependence of soil respiration. *Funct. Ecol.* 8, 315-323.
- Michaelis, L., Menten, M.L., 1913. Die Kinetik der Invertinwirkung. *Biochem. Z.* 49, 333.
- Moncrieff, J.B., Mahli, Y., Leuning, R., 1996. The propagation of errors in long term measurements of land atmosphere fluxes of carbon and water. *Global Change Biol.* 2, 231-240.
- Ruimy, A., Jarvis, P.G., Baldocchi, D.D., Saugier, B., 1995. CO₂ fluxes over plant canopies and solar radiation: a review. *Adv. Ecol. Res.* 26, 1-63.
- Saigusa, N., Oikawa, T., Liu, S., 1998. Seasonal variations of the exchange of CO₂ and H₂O between a grassland and the atmosphere: An experimental study. *Agric. For. Meteorol.* 89, 131-139.
- Schmid, H.P., Grimmer, C.S.B., Copley, F., Offerle, B., Su, H.B., 2000. Measurements of CO₂ and energy fluxes over a mixed hardwood forest in the mid-western United States. *Agric. For. Meteorol.* 103, 357-374.

Sims, P.L., Bradford, J.A., 2001. Carbon dioxide fluxes in a southern plains prairie. *Agric.For. Meteorol.* 109, 117-134.

Smith, E., 1938. Limiting factors in photosynthesis: light and carbon dioxide. *Gen. Physiol.* 22, 21–35.

Svejcar, T.J., Browning, J.A., 1988. Growth and gas exchange of *Andropogon gerardii* as influenced by burning. *J. Range Manage.* 41, 239-244.

Valentini, R., Matteucci, G., Dolman, A.J., Schulze, E.-D., Rebmann, C., Moors, E.J., Granier, A., Gross, P., Jensen, N.O., Pilegaard, K., Lindroth, A., Grelle, A., Bernhofer, C., Grünwald, T., Aubinet, M., Ceulemans, R., Kowalski, A.S., Vesala, T., Rannik, Ü., Berbigier, P., Loustau, D., Gu g mundsson, J., Thorgeirsson, H., Ibrom, A., Morgenstern, K., Clement, R., Moncrieff, J., Montagnani, L., Minerbi, S., Jarvis, P.G., 2000. Respiration as the main determinant of carbon balance in European forests. *Nature* 404, 861–865.

Webb, E.K., Pearman, G.I., Leuning, R., 1980. Correction of flux measurements for density effects due to heat and water vapor transfer. *Quart. J. R. Meteorol. Soc.* 106, 85-100.

Chapter 4 Modelling

Table of Content

4.1 Introduction.....	44
4.1.1 Global processes	44
Photosynthesis	44
Dark respiration	45
Photorespiration.....	46
Soil respiration.....	46
Plant categories.....	46
Stomata	46
4.1.2 Terminology.....	47
4.2 Models presentation	48
4.2.1 Collatz's Model	48
Assimilation.....	48
Temperature response.....	49
Stomatal conductance	49
4.2.2 Jacobs or A-g _s Model.....	50
Assimilation.....	51
Temperature response.....	52
Stomatal conductance	53
4.3 Calibration	54
4.3.1 Collatz's model.....	55
4.3.2 Jacobs' model.....	56
4.4 Modelling results and comparisons	57
4.4.1 Half-hour average flux	58
4.4.2 Daily flux	60
4.4.3 Monthly flux.....	60
4.4.4 Cumulative photosynthesis & global uptake	62
References.....	65

4.1 Introduction

In previous chapters, the data collection and presentation have been described for the Dripsey site during the study period. This data is precious for the time being and for the future, since they play a part at two levels. On the one hand, they illustrate the main plant mechanisms involved in the CO₂ budget, and their interactions. Models can then describe those processes and adjusted to fit each specific environment. On the other hand, they constitute a basis to compare and adjust variables in order to describe faithfully the reality. With all the climatic issues at present, more accurate predictions of the effect of changes due to CO₂ increasing concentration, or any other variable (precipitation, air temperatures....) on an ecosystem are needed.

In this study, modelling tools will only be discussed as an effort to describe accurately the site, and to fit as well as possible CO₂ flux fluctuations during the year.

A wide range of models is nowadays available to estimate the exchange between leaves and the atmosphere in terms of CO₂. Biochemical models as proposed by Farquhar *et al.* (1980) consider the full biochemical components of photosynthetic carbon assimilation in plants and therefore need a large number of physiological parameters that are not trivial to determine. On the other hand, empirical models, for the stomata conductance calculation, introduced by Jarvis (1976), and then by the widely used Ball-Berry model (1987), require few parameters but ignore well-known mechanisms. Models proposed by Collatz *et al.* (1991) and Jacobs (1994) are semi-empirical models combining the two approaches. Thus, they require relatively few parameters and retain the mechanisms of assimilation. A brief presentation of the plant physiological background, of those two models will be presented in detail and applied to our study.

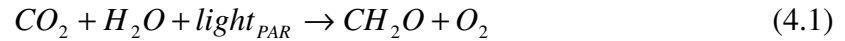
4.1.1 Global processes

Photosynthesis

The photosynthesis of green plants is a highly complicated set of interactive reactions in which the energy of light is trapped and used to convert CO₂ into carbohydrates ((CH₂O)_n). Two groups of reactions can be distinguished: the light reactions and the dark reactions.

In the light reactions, solar energy is trapped and stored into carriers of chemical energy. Only light in the visible wavelength (400 nm to 700 nm) is utilized. Solar radiation in this part of the spectrum may be referred to as Photosynthetically active radiations (PAR).

During the dark reactions, the light trapped in the light reactions is converted from CO_2 to carbohydrates. The most important pathway of the dark reaction is the so-called Calvin cycle. The first step in this chain of reactions is the fixation of CO_2 , which is catalysed by the enzyme ribulose 1,5 bi-phosphate carboxylase oxygenase, Rubisco (Campbell & Norman, Environmental Biophysics). The subsequent steps result in the formation of the required carbohydrate products. The complete set of light and dark reactions results in general reaction:



The ratio of the number of fixed CO_2 molecules (or O_2 produced) to the amount of photons used is called the quantum efficiency. The quantum efficiency near zero light intensity (the initial quantum use efficiency ϵ) is an important parameter in photosynthesis models because it determines the initial slope of the light response curve.

During photosynthesis, CO_2 passes through the intercellular spaces and enters the chloroplasts in the leaf mesophyll cells (Figure 4.1) where the carboxylation (transformation into an organic carbon product) occurs.

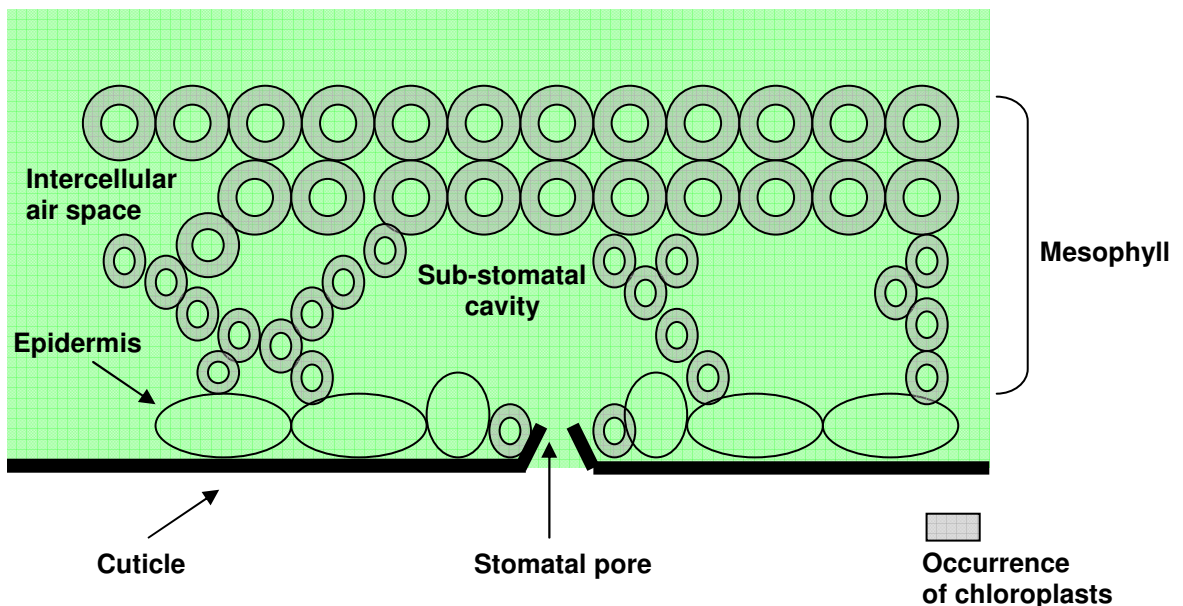


Figure 4.1: Structure of a leaf from Jacobs (1994)

Dark respiration

Part of the fixed carbon is used as an energy source for plant processes and as material to build structural dry matter. These mechanisms all result in the release of CO_2 . They are considered together under the name of dark respiration, because it takes place in the dark. There are indications that dark respiration in leaves is suppressed by light (Graham, 1979). The equation is the counter reaction of photosynthesis.

Photorespiration

Because the carbon fixing enzyme of the Calvin cycle, Rubisco, is not only a carboxylase but also an oxidase, CO_2 and O_2 compete for the same active site of Rubisco. Therefore, photosynthesis will be inhibited in the presence of O_2 . At the same time the oxidase activity of Rubisco will trigger a process that depends on the availability of light and ultimately result in the release of previously fixed CO_2 . This process is called photorespiration. C_3 plants may lose up to 50 % of the newly fixed CO_2 by photorespiration. No clear function has been yet identified for this mechanism so that it is often considered as a waste of energy.

Soil respiration

This release of CO_2 corresponds to the plant root respiration and decomposition of organic matter by micro-organisms.

Plant categories

Most plant species fall into one of the two major groupings with respect to carbon assimilation. In the most common group, the primary product of photosynthesis is a three carbon sugar. So these species are called C_3 plants. The CO_2 is directly introduced into the Calvin cycle.

A less common photosynthetic mechanism is present in tropical grasses and a number of important and productive crop species. In these the first product of photosynthesis is a four carbon compound. These species are therefore called C_4 plants. The fixing of CO_2 into the four carbon compound in C_4 species concentrates the carbon dioxide and minimizes photorespiration. The concentration of CO_2 inside the stomata of leaves is therefore much lower in C_4 than C_3 species typically resulting in higher photosynthetic rates and higher water use efficiency.

In our case, the metabolic pathway for carbon fixation is assumed to be a C_3 Cycle.

Stomata

The full mechanisms, which control stomata aperture, remain unknown. However, it has been demonstrated that the stomata are sensitive to the intercellular concentration of CO_2 , C_i , (and not to the concentration outside the leaf or inside stomatal pores) and is influenced by light, leaf temperature, air humidity and soil water content as well. Generally stomata close in the darkness and open if exposed to light. Higher temperatures increase the speed of stomatal movements and the final aperture. Moreover, stomata tend to close if the vapor pressure deficit of the surrounding air increases, and in response to the drying of soil. In that later case, closure starts only if the soil water potential drops down to rather low values.

4.1.2 Terminology

Regarding the CO₂ budget, fluxes have to be described separately for the plant and the ecosystem. Let P_p be the plant photosynthetic flux, R_p the plant respiration and R_s the soil respiration. Then R_e , the ecosystem respiration is defined as $R_e = R_s + R_p$. The net primary productivity (NPP) for the plant is the quantity of CO₂ absorbed when all processes have been taken into account:

$$NPP = P_p - R_p \quad (4.2)$$

At the scale of the whole ecosystem, the soil respiration must be added for the net ecosystem productivity (NEP):

$$NEP = NPP - R_s = P_p - R_p - R_s = P_s - R_e \quad (4.3)$$

The NPP for each part of the plant depends on the efficiency of growth

At the leaf level, the net assimilation, A_n , is balanced between the amount of carbon fixed by photosynthesis (the gross assimilation rate A_g) and the losses due to the dark respiration R_d :

$$A_n = A_g - R_d \quad (4.4)$$

The compensation point, Γ , is defined as the CO₂ concentration at which no assimilation occurs (Farquhar, 1980). In the absence of 'dark respiration', that means at light time, Γ increases linearly with the oxygen concentration in air (210000 $\mu\text{mol/mol}$), so that the light compensation point Γ^* can be written:

$$\Gamma^* = \frac{C_{oa}}{2\tau} \quad (4.5)$$

with τ the ratio describing the partitioning between carboxylase and oxygenase reactions of Rubisco.

The common way of expressing the total leaf area in a forest canopy or any other vegetation type is to use the leaf area index (LAI). It is the leaf surface per square meter ground surface. It is expressed in m^2/m^2 and allows the scaling up of leaf processes to a whole canopy.

The senescence is a productive form of aging leading to plant death. Plants age productively; as tissues senesce they produce enzymes necessary to recycle "expensive" materials and reroute the subunits to areas for use by active growth elsewhere, in the next season, or by the next generation. This process is responsible for the decrease in LAI in autumn.

4.2 Models presentation

4.2.1 Collatz's Model

Assimilation

The photosynthesis part of the Collatz 's model is an adaptation from Farquhar (1980), which describes the functioning of the biochemical components of photosynthetic carbon assimilation in C₃ plants (Campbell & Norman). Three limitations bound the assimilation rate (μmol/m²/s): light, CO₂ and export of products of photosynthesis. The light-limited assimilation can be computed from:

$$J_e = \frac{\alpha_{PAR} \times e_m \times Q_p \times (C_i - \Gamma^*)}{C_i + 2\Gamma^*} \quad (4.6)$$

where α_p is the absorptivity of the leaf for PAR, e_m the maximum quantum efficiency (maximum number of CO₂ molecules fixed per quantum of radiation absorbed), Q_p is the PAR photon flux density incident on the leaf (μmol/m²/s), C_i the intercellular CO₂ concentration (see equation 4.15) and Γ^* the light compensation point.

The Rubisco-limited assimilation rate is:

$$J_c = \frac{V_m \times (C_i - \Gamma^*)}{C_i + K_c \times \left(1 + \frac{C_{oa}}{K_o}\right)} \quad (4.7)$$

where V_m is the maximum Rubisco capacity per unit leaf area (μmol/m²/s), K_c is the Michaelis constant for CO₂ fixation and K_o is the Michaelis constant for oxygen inhibition.

The final limiting rate is controlled by the export and use of products of photosynthesis. When Sucrose builds up, the photosynthesis slows. It is considered as the most likely rate-limiting step. The sucrose-limited assimilation is assumed, by Collatz *et al.* (1991) to be just:

$$J_s = \frac{V_m}{2} \quad (4.8)$$

The gross assimilation rate then is the minimum of those limiting-rates.

$$A_g = \min[J_e, J_c, J_s] \quad (4.9)$$

The net assimilation A_n is deduced from equation (4.9) minus the dark respiration.

$$A_n = A_g - R_d \quad (4.10)$$

Temperature response

The dark respiration, as well as some other parameters of the model needs a temperature adjustment. For K_c , K_o and τ the temperature dependence is an exponential relationship normalized with respect to 25°C (see equation 4.11) whereas, for V_m and R_d , a high temperature cut-off is needed (see equations 4.12 & 4.13).

$$X(T) = X(@ 25)e^{q \times (T-25)} \quad (4.11)$$

where q is the temperature coefficient for the parameter X and $X(@25)$ its value at 25°C.

$$V_m = \frac{V_{m,25} \times e^{0.088 \times (T-25)}}{1 + e^{0.29 \times (T-41)}} \quad (4.12)$$

$$R_d = \frac{R_{d,25} \times e^{0.069 \times (T-25)}}{1 + e^{1.3 \times (T-55)}} \quad (4.13)$$

Stomatal conductance

Knowing the net assimilation, the stomatal conductance is deduced thanks to the empirical formula from Ball *et al.* (1987):

$$g_s = \frac{m \times A_n \times h_s}{C_s} + b_{gs} \quad (4.14)$$

where m and b_{gs} are constant, h_s is the humidity at leaf surface (which is assumed to be air humidity) and C_s the CO₂ concentration at leaf surface.

The third equation used to solve the $C_i / A_n / g_s$ system is the Fick's Law of diffusion applied to CO₂.

$$C_i = C_s - \frac{A_n}{g_s} \quad (4.15)$$

It has been assumed here that C_s is equal to C_a the atmospheric CO₂ concentration (380 ppm).

Equations (4.9), (4.14) and (4.15) constitute the core of the model as the description of interactions between the internal concentration of CO₂, the net assimilation and the stomatal conductance. Being interdependent, they need to be solved simultaneously. The program codes can be seen on Appendix 2.1.

In the light of those equations, this model has few inputs (PAR radiation, air temperature, and air humidity) but about fifteen parameters depending on the plant type. The full list of values chosen in our case is given in Appendix 1. However, considering the works done by Collatz *et al.* (1991), Ball *et al.* (1987) and more specially Farquhar *et al.* (1980) as for C₃ grass, only a few of those parameters have been tested for calibration in this study. The calibration procedure described in the paragraph 4.3, concentrates on the six parameters that vary most likely from one site to another.

4.2.2 Jacobs or A-g_s Model

Based on the empirical model from Jarvis (1976) for the stomatal conductance, the A-g_s model uses the model from Goudriaan *et al.* (1985) to describe the photosynthesis part. Goudriaan's model describes most of the essential characteristics of photosynthesis. It is less detailed than Farquar's model and therefore needs less input parameters. This model is often linked to meteorological research (see Calvet *et al.*, 1998 & 2001).

A correct model for stomatal behaviour must be able to include the effect of short-term variations (light, temperature) as well as long-term changes (increase of atmospheric CO₂). The effects of those factors are combined, since it is known for instance that an increase of atmospheric CO₂ increases the plant sensitivity to light and temperature and possibly to other factors too (Meidner & Mansfield, 1968). However, Jarvis' model, frequently used in meteorological research, does not take into account synergistic effects between different stimuli. The alternative used in A-g_s is based on the observed correlation between the photosynthetic rate A, and the stomatal conductance. At the cost of increased complexity, the responses to CO₂ are described including interactions between stimuli. Moreover, this model may be expected to be more generally applicable since relying more on the very nature of plants and less on statistics.

In Goudriaan *et al.* (1985) photosynthetic rate does not only depend on the biochemical processes of photosynthesis. The diffusion process which controls the transport of CO₂ from the atmosphere to the carboxylation sites inside the leaf, sets a physical limit to the photosynthetic rate and is controlled by many conductances. Some of these conductances are physical in nature. Others are related to chemical processes and are called 'conductance' to allow a convenient comparison of limitations imposed by chemical and physical processes. See figure 4.1 for location of conductances described here:

- The stomatal conductance (g_{sc} for CO₂ and g_s for vapor water) describes the diffusion through stomata pores. The difference in diffusivity has to be accounted for so that $g_s = 1.6 \times g_{sc}$.
- The cuticular conductance describes the diffusion of water and CO₂ through the waxy cuticle. For convenience, g_c is usually assumed the same for water and CO₂. The total conductance through epidermis (see Figure 4.1) can be calculated as $g_{epidermis} = g_s + g_c$ for water and with g_{sc} instead of g_s for CO₂. When stomata are widely open $g_c \ll g_s$, whereas g_c may become larger than g_s when they are closed.
- The mesophyll conductance (g_m), describes the transport of CO₂ between the sub-stomatal cavity and the site of carboxylation. g_m includes a variety of conductances from physical or chemical processes. Since, the values of the latter are not known for certain, g_m is treated as one residual resistance.

Assimilation

The modelling approach of A_g s, directly relies on conductances to describe the diffusion of CO_2 between the air and chloroplasts. It is based on the distinction between two different conditions:

- the light-limiting factor.
- the CO_2 limiting factor.

If light is the limiting factor, A_n can be written as:

$$A_n = \varepsilon \times I_a - R_d \quad (4.16)$$

where I_a is the amount of absorbed PAR radiation, R_d is the dark respiration and ε the initial quantum use efficiency. This latter parameter quantifies the slope of the light response curve, and is affected by photorespiration. It can be calculated as (Goudriaan *et al.*, 1985):

$$\varepsilon = \varepsilon_0 \times \frac{C_s - \Gamma}{C_s + 2\Gamma} \quad (4.17)$$

Γ is the compensation point (in ppm), C_i the internal concentration of CO_2 and ε_0 the maximum quantum use efficiency based on the theoretical efficiency of the Calvin cycle. Equation (4.17) is derived from biochemical considerations and is similar to the result obtained by Farquhar (1980).

In case that CO_2 is the only limiting factor, the photosynthetic rate at light saturation, A_m , is linearly related to the CO_2 concentration.

$$A_m = 0.001 \times g_m \times (C_i - \Gamma) \times \varphi_c \quad (4.18)$$

Putting together equations (4.16) and (4.18), the final expression for A_n including both the effect of limited light and CO_2 is:

$$A_n = (A_m + R_d) \times \left(1 - e^{\frac{-\varepsilon \times I_a}{A_m + R_d}} \right) - R_d \quad (4.19)$$

Here, the respiration rate R_d is simply defined as $R_d = \frac{A_m}{9}$. (4.20)

In order to bound the photosynthetic rate at high light intensities and high CO_2 concentrations, A_m must be limited to a maximum value $A_{m,max}$. A smooth transition between equation (4.18) and $A_{m,max}$ is provided with:

$$A_m = A_{m,max} \times \left(1 - e^{\frac{-0.001 \times g_m \times (C_i - \Gamma) \times \varphi_c}{A_{m,max}}} \right) \quad (4.20)$$

A_n and A_m are calculated here in $\text{mg/m}^2/\text{s}$, g_m is in mm/s and the concentrations are in ppm ($\mu\text{mol/mol}$). φ_c is simply a conversion factor transforming ppm to mg/m^3 .

$$\varphi_c = \frac{M_{\text{CO}_2} \times \rho_{a,v}}{M_a} \quad (4.21)$$

where M_{CO_2} and M_a are the molecular masses of CO_2 and air (44 and 28.9 g/mol respectively), and ρ_a the density of air calculated thanks to the vapor content

$$\rho_{a,v} = \frac{P}{R_a \times T \times \left(1 + \left(\frac{R_v}{R_a} - 1 \right) \times \frac{q}{1000} \right)} \quad (4.22)$$

where R_v and R_a are the gas constants for air and vapor pressure, P is the air pressure in Pa, T the air temperature (in K) and q the specific air humidity in kg/kg .

Temperature response

As for Collatz *et al.* (1991), the temperature dependence of photosynthesis is accounted for through the temperature dependence of several parameters. The response of those variables is based on a Q_{10} function, which is a proportional increase of a parameter for a 10°C increase in temperature (Berry & Raison, 1982). For Γ , the equation (4.23) is used whereas for g_m and $A_{m,\text{max}}$, the function is modified using an inhibition expression (equation (4.24)).

$$X(T) = X(@25) \times Q_{10}^{\frac{T-25}{10}} \quad (4.23)$$

$X(T)$ is the value of any variable X at the temperature, with a reference value $X(@25)$ at 25°C .

$$X(T) = \frac{X(@25) \times Q_{10}^{\frac{T-25}{10}}}{\left(1 + e^{0.3(T_1-T)} \right) \times \left(1 + e^{0.3(T_2-T)} \right)} \quad (4.24)$$

T_1 and T_2 denote reference temperature, which can be adjusted to mimic species-specific features.

The reference values have been adapted from Jacobs (1994) and Bruse (2001). The calibration process will be discussed in paragraph 4.3 and the full list of parameter can be found in Appendix 1.

Stomatal conductance

The effect of humidity on the stomatal response, and internal CO₂ concentration is parameterised thanks to a factor f defined as:

$$f = f_0 \times \left(1 - \frac{D_s}{D_{\max}}\right) + f_{\min} \times \left(\frac{D_s}{D_{\max}}\right) \quad (4.25)$$

D_s is the vapor pressure deficit of air at the plant surface in g/kg and D_{\max} is its maximum value. f_0 is the value of f for $D_s = 0$ g/kg which is around 0.85 for C₃ plants. The minimum f_{\min} is calculated with equation (4.26).

$$f_{\min} = \frac{g_c}{g_c + g_m} \quad (4.26)$$

where g_c is the cuticular conductance and g_m the mesophyll conductance.

The internal CO₂ concentration, C_i , is then obtained from f , and the value of CO₂ concentration at leaf surface:

$$C_i = f \times C_s + (1 - f) \times \Gamma \quad (4.27)$$

Considering A_g the gross assimilation rate defined in equation (4.4) and $A_{m,g}$ the gross assimilation at light saturation, the stomatal conductance g_{sc1} (m/s) of the leaf for CO₂ transfer can be calculated as

$$g_{sc} = \frac{A_n - A_{\min} \times \frac{D_s \times A_g}{D_{\max} \times A_{mg}} + R_d \times \left(1 - \frac{A_g}{A_{mg}}\right)}{(C_s - C_i) \times \varphi_c} \quad (4.28)$$

where A_{\min} is the value of A_m for $C_i = C_{\min}$ in equation (4.18) and C_{\min} is given below:

$$C_{\min} = \frac{g_s \times C_s + g_m \times \Gamma}{g_c + g_m} \quad (4.29)$$

The total leaf stomatal conductance for vapor, including the cuticular conductivity can then be deduced from equation (4.30).

$$g_s = 1.6 \times 1000 \times g_{sc} + g_c \quad (4.30)$$

This model is closely linked up with micrometeorological research practice. The description remains simple, but effective in its simulation of most of the well-known features of photosynthesis. As well as for Collatz's model, few inputs are needed: PAR radiation, air temperature, air humidity, and atmospheric pressure. However, less parameters are needed here than for the former model.

The full list of values chosen in our case is given in Appendix 1. However, the parameters are tuned to the results of the biochemically based models (Farquhar *et al.*; 1980), so that general values for C₃ grass are used here and only a few has been specifically calibrated.

4.3 Calibration

The two sets of equations in the former paragraph (from equation (4.6) to equation (4.15) and from (4.16) to (4.30)) model photosynthesis processes at leaf scale. In order to find the parameters that best describe the vegetation and climate of the Dripsey site, we compared Collatz's and Jacobs' models to the measurements made by the weather station, during the study period. To do so we needed to work on the same scale for measured and modelled values. The scaling up from leaf to canopy for both models is obtained by a simple multiplication by the assumed LAI for the site.

The LAI has not been measured and consequently has been assumed for this study at the constant value LAI=1.5. Moreover, the available light is not the same between the bottom and the top of the canopy. The radiation is attenuated as a function of the LAI, so that young grass near the ground receives a smaller photosynthetic photon flux. The rate of decrease is generally considered as an exponential decay.

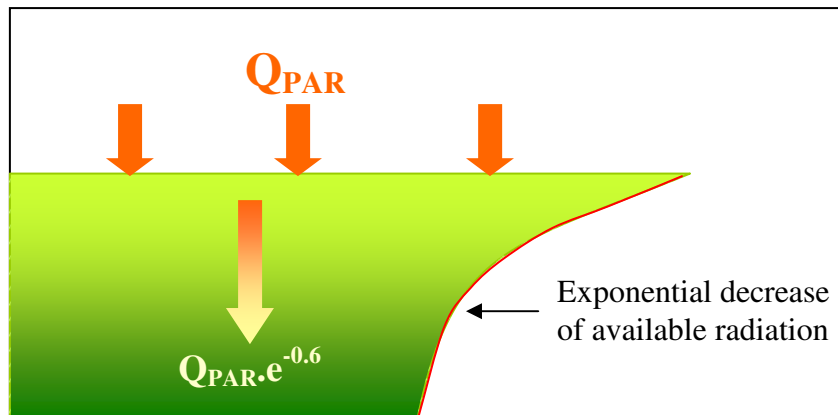


Figure 4.2: Light extinction in the canopy

Considering the small complexity of the grassland field in comparison with canopy systems such as forests, an average value of the photon flux received at the top and at the bottom of the canopy has been applied uniformly. The PAR radiation input for modelling becomes:

$$Q = Q_{PAR} \times \frac{(1 + e^{(-0.4 \times LAI)})}{2} \quad (4.31)$$

where Q_{PAR} is the measured incoming photon flux in the PAR wavelength from the weather station.

The calibration of each model has been carried out thanks to a sensitivity analysis for the most varying parameters. The suitability of each set of values has been analysed for different time scales by the mean of typical error measurements. Those latter compare observed and modelling fluxes. Three definitions of error were applied to the 30 minutes averaged flux, to the daily flux, to the monthly flux, to the 30 minutes averaged photosynthetic flux, and to the cumulative photosynthetic flux: the R^2 error, the mean average error (MAE), and the root mean square error (RMSE). The study of the bias was added for the cumulative uptake over the year of study. Equations from (4.32) to (4.35) give a definition of each error for a given measured flux (F_{observed}) and a modelled flux (F_{modelled}).

$$R^2 = 1 - \frac{\text{var}(F_{\text{observed}} - F_{\text{modelled}})}{\text{var}(F_{\text{observed}})} \quad (4.32)$$

$$MAE = \frac{1}{n} \sum_{i=1}^n |F_{\text{observed}}(i) - F_{\text{modelled}}(i)| \quad (4.33)$$

$$RMSE = \sqrt{\left(\frac{1}{n} \times \sum_{i=1}^n (F_{\text{observed}} - F_{\text{modelled}})^2 \right)} \quad (4.34)$$

$$Bias = \frac{1}{n} \sum_{i=1}^n (F_{\text{observed}} - F_{\text{modelled}}) \quad (4.35)$$

4.3.1 Collatz's model

This model has a great number of parameters. In order to reduce the computation time of the sensitivity analysis, most parameters were held at the value defined by Farquhar (1980) for C_3 grass (Appendix 1). In this study, attention has been focused on parameters that were usually different from one site to another or from one type of grass to another (see values given by Collatz for C_4 grass and by Farquhar for C_3 grass in Appendix 1). Moreover, some temperature dependent variables such as τ or K_o , and K_c are defined by two coefficients: X (@25°C) and q_X the temperature coefficient. In that case, values at 25°C were directly applied without any change. Only the temperature coefficients were analysed. We ended with a set of four parameters for the sensitivity analysis: q_{K_o} , q_{K_c} , q_τ and m from the stomatal conductance equation (4.14). Table 4.1 gives for each error definition and at each time scale, the best set of the four studied parameters, as well as the associated error value.

This calibration is just the first step at our site. A more detailed analysis should be done when the values of the seasonal variability of the leaf area index (LAI) for the site will be known.

<i>Collatz</i>	q_{K_o}	q_{K_c}	q_{τ}	m	Errors
30 minutes averaged fluxes					
R^2	0.055	0.075	-0.02	5.75	0.7753
MAE	0.045	0.065	-0.02	6	1.6873
RMSE	0.055	0.075	-0.02	5.75	2.7975
Daily fluxes					
R^2	0.04	0.075	-0.02	5.75	0.5882
MAE	0.04	0.065	-0.02	5.75	3.6375
RMSE	0.05	0.075	-0.02	5.75	5.0656
Monthly fluxes					
R^2	0.045	0.095	-0.02	5.75	0.948
MAE	0.05	0.085	-0.02	6.75	42.4723
RMSE	0.045	0.075	-0.02	6.75	50.3415
30 minutes averaged Photosynthesis flux					
R^2	0.05	0.075	-0.02	6.25	0.627
MAE	0.05	0.065	-0.02	6.75	2.7788
RMSE	0.055	0.075	-0.02	6.5	3.7296
Cumulative photosynthesis					
R^2	0.05	0.065	-0.02	6.75	0.9984
MAE	0.04	0.065	-0.02	6.75	0.1722
RMSE	0.045	0.065	-0.02	6	0.2105
Cumulative net assimilation					
R^2	0.05	0.075	-0.02	6.75	0.9799
MAE	0.05	0.075	-0.025	5.75	0.1265
RMSE	0.05	0.075	-0.025	5.75	0.1559
Bias	0.045	0.075	-0.02	6	0.0014

Table 4.1: Final result of the parameters calibration for Collatz's model

Considering, the results given in Table 4.1, each factor seems relatively bounded. Manual calibrations have been run then to obtain globally satisfactory results. The chosen values for those parameters are:

$$\begin{array}{ll}
 q_{K_o} = 0.05 & q_{K_c} = 0.07 \\
 q_{\tau} = -0.02 & m = 6.75
 \end{array}$$

Those results are consistent with usual values for such coefficients. They are used for the following part (paragraph 4.4) on CO₂ fluxes analysis.

4.3.2 Jacobs' model

As it has been seen earlier, Jacobs' model has less parameters than Collatz's model. However, in order to optimise the computation time for the sensitivity analysis, only four of them have been studied here. The other parameters were held at the value given by Jacobs (1994) for C₃ grass (see Appendix 1). The temperature dependent variables are defined thanks to two coefficients each: the value at 25°C (X (@25°C)) and a temperature coefficient $Q_{10}(X)$. As for the previous model, X

(@25°C) were assumed to fit the observations and therefore were not changed, except for A_{m_max} @ 25°C which changed from 2.2 to 2.4 mg/m²/s after a preliminary analysis. Table 4.2 gives for each error definition and each time step, the best set for f_o , $Q_{10}(\Gamma)$, $Q_{10}(A_{m,max})$ and $Q_{10}(g_m)$, as well as the associated error value.

We notice from Table 4.2 that f_o is the most sensitive parameter. It fluctuates a lot within the same time scale but for different error definitions. This can be explained by the direct impact of this variable on the intercellular CO₂ concentration and consequently on the flux. On the opposite, $Q_{10}(\Gamma)$ is surprisingly constant at the value 0.8. Nevertheless, this value is supposed, in literature, to be greater than one, for Γ increases as temperature increases. With our value of 0.8 the behaviour of the Γ function is set to the opposite (decreases as temperature increases). Manual calibrations were then carried out to find a more reliable value for $Q_{10}(\Gamma)$, which changes as little as possible the other parameters and still gives us good visual results.

$$\begin{array}{ll} f_o = 0.94 & Q_{10}(\Gamma) = 1.2 \\ Q_{10}(A_{m,max}) = 1.6 & Q_{10}(g_m) = 1.6 \end{array}$$

Those results are used for the modelled CO₂ flux analysis.

Jacobs	f_o	$Q_{10}(\Gamma)$	$Q_{10}(A_{m,max})$	$Q_{10}(g_m)$	Errors
30 minutes averaged fluxes					
R ²	0.825	0.8	1.6	2.8	0.6504
MAE	0.905	0.8	1.6	2.4	2.2336
RMSE	0.825	0.8	1.6	2.8	3.4923
Daily fluxes					
R ²	0.91	0.8	1.6	2.4	0.23
MAE	0.92	0.8	1.2	2.4	5.3817
RMSE	0.875	0.8	1.6	2.4	6.9635
Monthly fluxes					
R ²	0.92	0.8	1.2	1.6	0.9129
MAE	0.93	0.8	1.6	0.8	45.5761
RMSE	0.935	0.8	1.6	0.8	54.2776
30 minutes averaged Photosynthesis flux					
R ²	0.89	0.8	1.6	2.4	0.4266
MAE	0.94	0.8	1.6	1.6	3.4639
RMSE	0.89	0.8	1.6	2.4	4.6198
Cumulative photosynthesis					
R ²	0.94	0.8	1.6	0.8	0.9987
MAE	0.94	0.8	1.6	0.8	0.1536
RMSE	0.94	0.8	1.6	0.8	0.1839
Cumulative net assimilation					
R ²	0.93	0.8	1.6	0.8	0.9806
MAE	0.93	0.8	1.6	0.8	0.1102
RMSE	0.93	1.4	1.6	1.6	0.1425
Bias	0.845	1	2.4	1.6	2.16E-05

Table 4.2: Final result of the parameters calibration for Jacobs' model

Modelling results and comparisons

The following analysis examines the results of the Collatz model and Jacobs model for increasing time scales. The smallest time scale of 30 minutes averaged flux is first examined, then the daily flux and monthly flux. Finally, a comparison of the Collatz and Jacobs cumulative flux in terms of global uptake and photosynthesis was performed. For simplicity, let MC be the Collatz' model and MJ be the Jacobs' model.

4.4.1 Half-hour average flux

Figures 4.3 (a) & (b) show F_{30} (the 30 minutes averaged CO_2 flux) over the whole study period for the Collatz and Jacobs models. The magnitude of F_{30} is respected for nighttime fluxes with values of about $5 \mu\text{mol}/\text{m}^2/\text{s}$ for both models. Nevertheless, each model reacts in a different way to the seasonality of the daytime F_{30} . MC's F_{30} decreases during the winter period (the second third of the study period) from about $14 \mu\text{mol}/\text{m}^2/\text{s}$ in the first third to $5 \mu\text{mol}/\text{m}^2/\text{s}$ in winter and then grows back again in the last third of the study period, whereas the observed F_{30} fluctuates on a greater range (between $2 \mu\text{mol}/\text{m}^2/\text{s}$ and $25 \mu\text{mol}/\text{m}^2/\text{s}$ see Chapter 3). MJ's F_{30} tracks the seasonality of the observed flux, but the transitions of autumn/winter and winter/spring are not well modelled (see Figure 4.3 (b)). For both models, the spring values are too small. In addition, MJ seems less stable than MC since from time to time MJ's F_{30} values show peaks much higher than the normal values. Those events happen more often at nighttime.

Figures 4.3 from (c) to (h) are specific periods to examine the behaviour of the models. For the three periods, August the 30th and September the 6th (c), November the 19th and November the 29th (e), and between June the 10th and June the 18th (h), both models simulate well the observed F_{30} . Those periods correspond to the end of summer 2001 before the senescence of plants, resting time in winter and beginning of summer 2002. Between September the 19th and September the 25th (d) (the beginning of the senescence), December the 15th and December the 23rd (f) (the lowest photosynthesis time), and between March the 24th and April the 3rd (g) (full springtime), MC and MJ are consistent with one another but differ from the observations. In spring and autumn ((d) & (g)) both models underestimate the observed F_{30} . In winter both models overestimate the photosynthetic flux by as much as a factor of six.

As both models are in general close during the whole study period, we can infer that they are calibrated on the same physical and biological basis. However MJ has a better understanding of factors driving the seasonality. The difference with the observed F_{30} is likely to be linked with the LAI definition in the models. Indeed, the LAI was supposed to be constant here since no measures can assess its real fluctuations. But with increasing values of LAI in spring and decreasing values in autumn, the modelled F_{30} should be higher in midseason and smaller in deep winter with smoother transitions between seasons.

— Collatz 's model flux
 — Jacobs' model flux
 — Observed flux

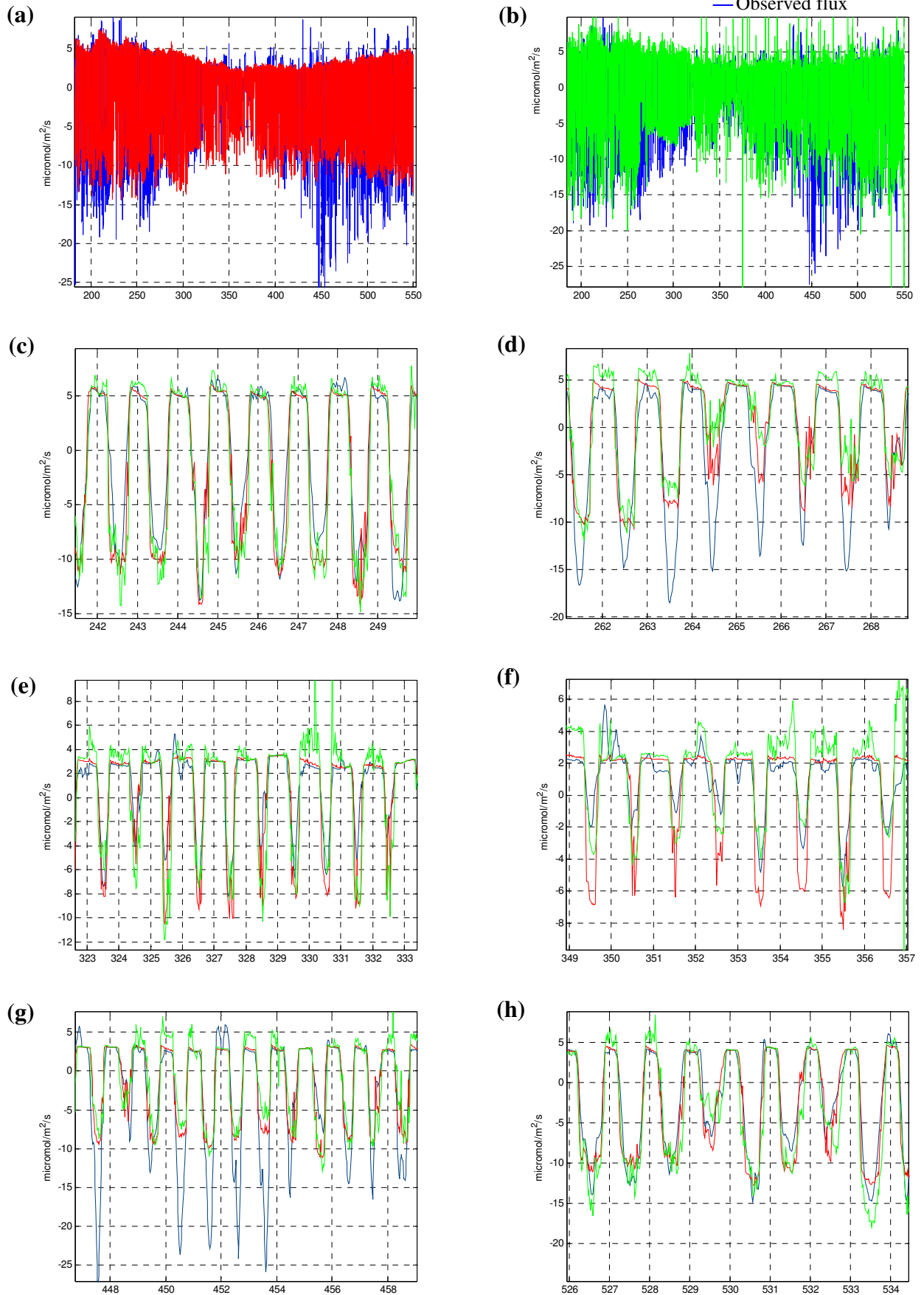


Figure 4.3: 30 min. average CO₂ flux (a) & (b) for the year of study, (c) 30th of Aug./6th of Sep., (d) 19th of Sep./25th of Sep, (e) 19th of Nov./ 29th of Nov., (f) 15th of Dec./23rd of Dec., (g) 24th of Mar./3rd of Apr., (h) 10th of Jun/18th of Jun.

4.4.2 Daily flux

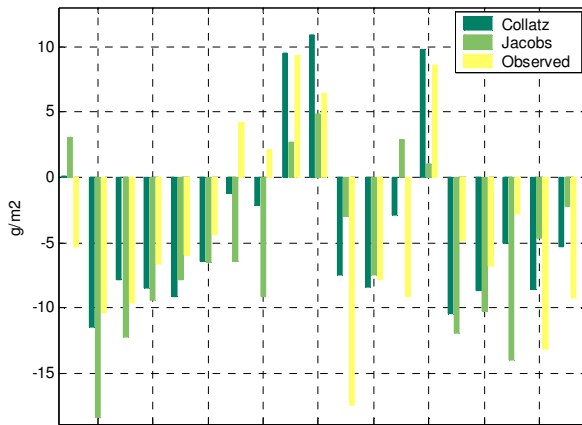
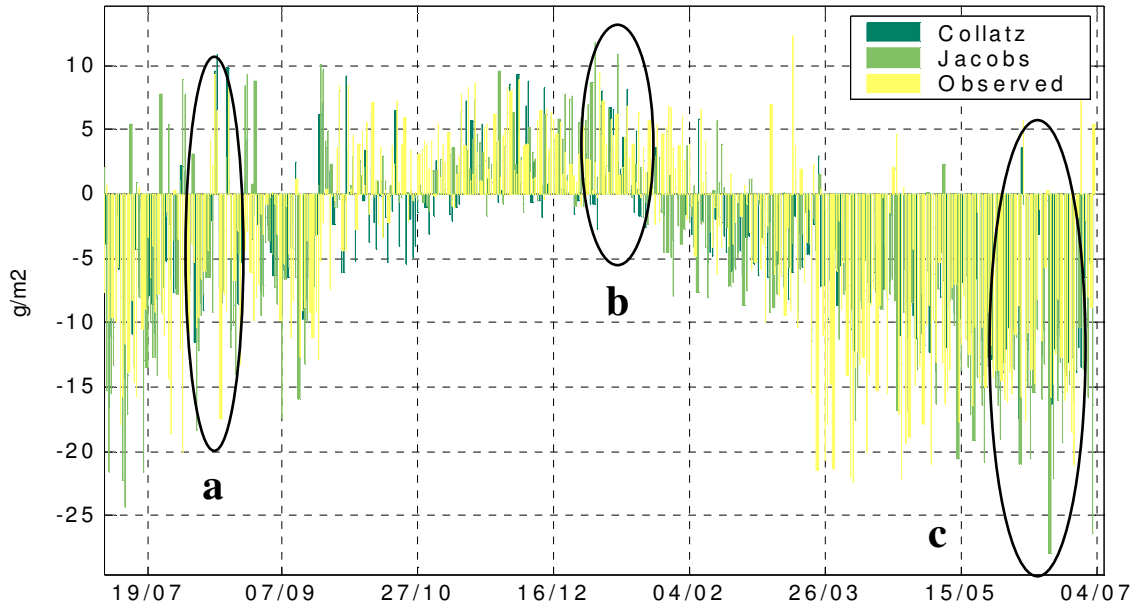
Figure 4.4 shows the daily CO₂ flux (F_d) for observed data, and both models, for three detailed sections (a), (b) and (c) centred on interesting events. The general trends for modelled F_d fit reasonably the observed. Yet, near October the 27th, where the daily flux becomes positive, we notice that MC is late in doing so. On the contrary both models are ahead of the observations regarding the transition between positive and negative fluxes around February the 2nd (b).

The selected section (a) underlines the accuracy of MC and MJ. In this global uptake period, even special days of release (either because of rain or clouds) are well predicted. So that external conditions are correctly taken into account. This is the case as well for section (c) for sudden release days. During those periods, one can notice that MJ is somehow late to react to such events being either smaller or staying negative. Section (c) displays some very good sets of days where models and observed value are very similar.

Because of the sudden peaks sometimes observed for MJ's F_{30} , the daily flux modelled by MJ is often greater than the observations. So that MC gives, for that time scale, more satisfactory results.

4.4.3 Monthly flux

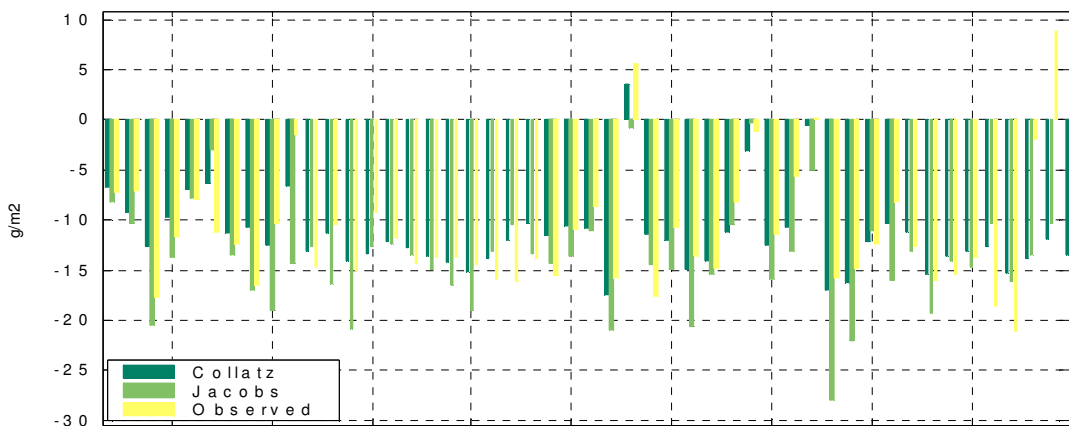
The monthly fluxes for MC and MJ are presented on figure 4.5. Here again, both models show a quicker decrease in autumn than the observations and a slower increase in spring. With this time scale, it is clear that the photosynthetic part is overestimated during the period as a source of CO₂, especially for MC. For MC the duration when the site behaves as a source of CO₂ is shorter, since this model is late to release carbon and returns to the sink state earlier. An interesting month is June 2002 since it emphasizes the lag effect between observed and modelled values. Whereas the highest month in terms of CO₂ uptake is May in the observations, MC and MJ still increase between May and June. Thus the shift between winter and summer is slower but longer in the modelling case. MJ shows extreme values for full winter in December with a release of 130 mg of CO₂ /m² for this month, and full summer in June with an uptake of 400 mg of CO₂ for this month. Few unstable and very high values over the time scale of 30 minutes can be responsible for high monthly values when summed up.



a



b



c

Figure 4.4. : Daily CO₂ flux for observed data, Collatz’s model & Jacobs model, (a), (b) and (c) are detailed sections from the top figure.

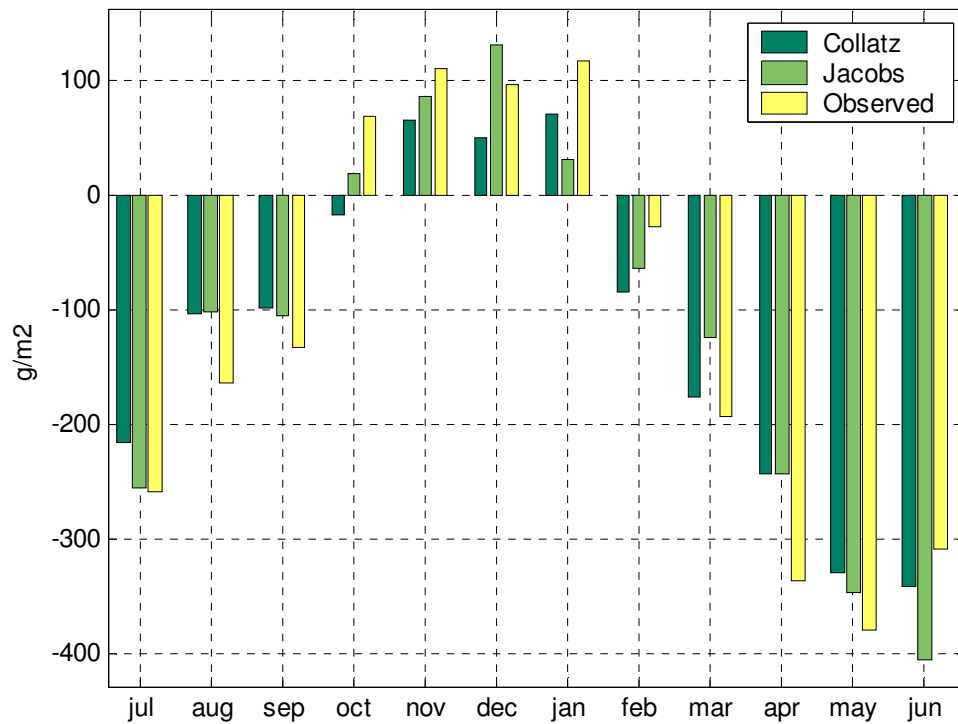


Figure 4.5: Monthly CO₂ flux for observed data, Collatz's model & Jacobs model.

4.4.4 Cumulative photosynthesis & global uptake

As seen in chapter 3, the cumulative quantities are very important for they represent in a striking way the main characteristics of a site and its capacity to act as a sink or a source of carbon. Having reasonably good results for the previous time scales, one can be confident in the acceptability of the cumulative fluxes be it the photosynthesis flux or the net uptake over the year of study. We believe this way of analysis to be reliable, for cumulative fluxes studied alone can lead to misunderstanding in calibration. Indeed, errors can cancel out.

Figures 4.6 & 4.7 depict the evolution of CO₂ and photosynthesis for Collatz's model and Jacobs' model in comparison with the observations. The photosynthetic part of the flux for MJ and to a lesser extend for MC are slight overestimations (Figure 4.7). The biggest difference is during the winter period where the photosynthesis has to be reduced to fit the observations. MC is very close to the observation and ends with the same cumulative uptake (by the photosynthesis process only) of 18 T of Carbon. As for the net uptake, both models simulate the main trend of the observed curve (with a slightly better shape for MJ) as well as the ending value around -3.9 T of Carbon for one year (Figure 4.6). This latter figure reveals an underestimation of the photosynthesis component or an overestimation of the respiration component when modelled curve exceed the observations. On the other hand an overestimation of the photosynthesis part is noticed when they stand below the observations. Consequently, by studying the slopes and the position of each curve, the same remarks as before can be made about the too quick autumnal decrease, the too slow springtime increase or the photosynthesis overestimation during wintertime.

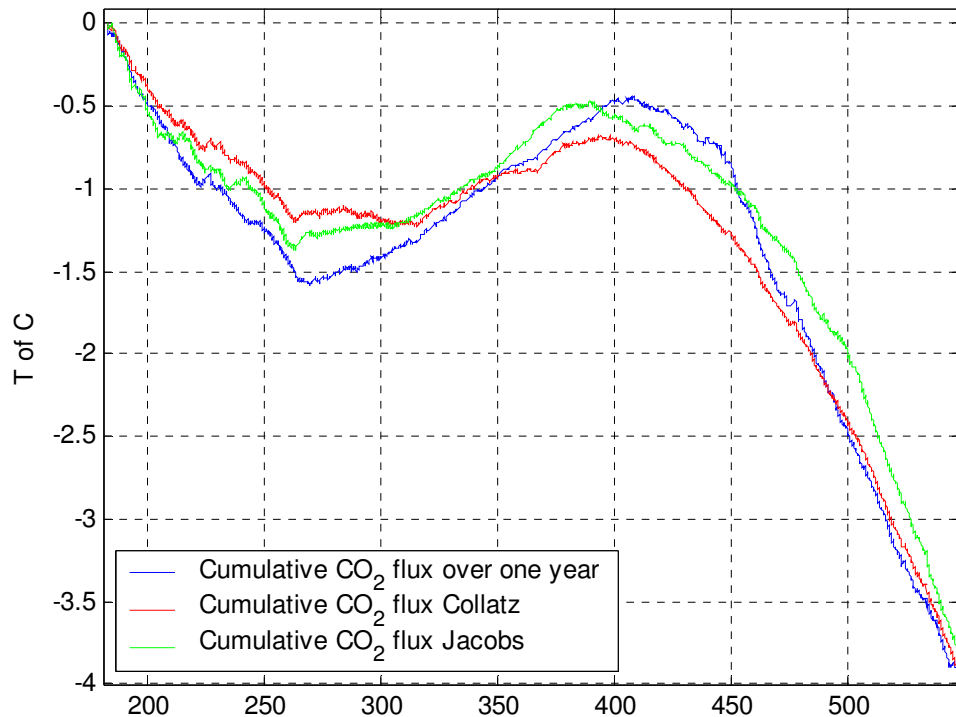


Figure 4.6: Comparison of the cumulative uptake of CO₂ over the year of study between the observed data and the two models.

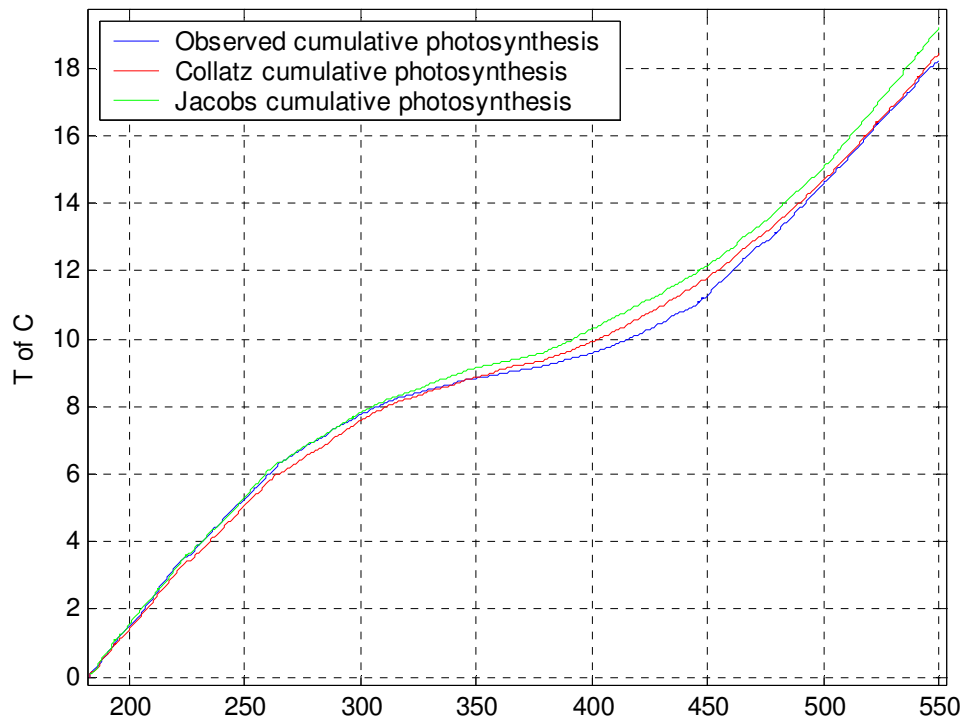


Figure 4.7: Comparison of the cumulative photosynthesis over the year of study between the observed data and the two models

In conclusion, Collatz's model and Jacobs' model give both satisfactory results on the different time scales. Jacobs' model is quicker to calibrate and simulates well the seasonal fluctuations. However it behaves in unstable ways from time to time, which bias slightly the daily and monthly fluxes. Collatz's model depicts well the photosynthesis process and gives good daily results. As for, the senescence and growing transition in autumn and spring, they will certainly be improved by a good definition of the LAI fluctuation during the year.

References

- Ball, J.T., Woodrow, I.E., Berry, J.A., 1987. A model predicting stomatal conductance and its contribution to the control of Photosynthesis under different environmental conditions. *Progress in Photosynthesis Research*. 4, 221-224.
- Berry, J.A., Raison, J.K., 1982. Responses of Macrophytes to temperature. In: Lange, O.L., Nobel, P.S., Osmond, C.B., Ziegler, H., *Encyclopedia of Plant Physiology*, New series, Vol. 12B, *Physiological Plant Ecology II*. Springer Verlag, Berlin, 277-338.
- Bruse, M., 2001. ENVI-met implementation of the Jacobs A-gs model to calculate the stomata conductance. Working paper.
- Calvet, J.C., Noilhan, J., Roujean, J.L., Bessemoulin, P., Cabelguenne, M., Olioso, A., Wigneron, J.P., 1998. An interactive vegetation SVAT model tested against data from six contrasting sites. *Agric. For. Meteorol.* 92, 73-95.
- Calvet, J.C., Soussana, J.F., 2001. Modelling CO₂ enrichment effects using an interactive vegetation SVAT scheme. *Agric. For. Meteorol.* 108, 129-152.
- Campbell, G.S., Norman, J.M. *An introduction to environmental biophysics*. Second Edition.
- Collatz, G.J., Ball, J.T., Grivet, C., Berry, J.A., 1991. Physiological and environmental regulation of stomatal conductance, photosynthesis and transpiration: a model that includes a laminar boundary layer. *Agric. For. Meteorol.* 54, 107-136.
- Collatz, G.J., Ribas-Carbo, M., Ball, J.A., 1992. Coupled photosynthesis-stomatal conductance model for leaves of C₄ plants. *Aust. J. Plant Physiol.* 19, 519-538.
- Farquhar, G.D., von Caemmerer, S., Berry, J. A., 1980. A biochemical model of photosynthetic CO₂ assimilation in leaves of C₃ species. *Planta*. 149, 78-90.
- Goudriaan, J., van Laar, H.H., van Keulen, H., Lovworse, W., 1985. Photosynthesis, CO₂ and plant production. In: Day, W. Day & R.K. Atkin (Eds.), *Wheat growth and modelling*. NATO ASI Series, Series A, Vol. 86. Plenum Press, New York, 107-122.
- Jacobs, C.M.J., 1994. Direct impact of atmospheric CO₂ enrichment on regional transpiration. Ph.D. Thesis. Agricultural University, Wageningen.
- Jarvis, P.G., 1976. The interpretation of leaf water potential and stomatal conductance found in canopies in the field. *Phil. Trans. R. Soc. London B*. 273, 593-610.
- Katul, G.G., Ellsworth, D.S., Lai, C.T., 2000. Modelling assimilation and intercellular CO₂ from measured conductance : a synthesis of approaches. *Plant, Cell, Environ.* 23, 1313-1328.
- Leuning, R., 1995. A critical appraisal of a combined stomatal-photosynthesis model for C₃ plants. *Plant, Cell Environ.* 18, 339-355.
- Lhomme, J.P., 2001. Stomatal control of transpiration : examination of the Jarvis-type representation of canopy resistance in relation to humidity. *Water Resour. Res.* 37, 689-699.
- Meidner, H., Mansfield, T.A., 1968. *Physiology of Stomata*, McGraw-Hill, London.
- Osborne, C.P., Woodward, F.I., 1999. *The MEDRUSH Vegetation Model*. Work Paper.

Chapter 5 Conclusion

5.1 Conclusion

The main conclusions brought out from the data analysis study deal with the importance of climate and land use management in CO₂ net exchange. A clement climate in terms of temperatures can delay the onset of the senescence and bring forward spring growth. So that, 30 minutes averaged fluxes or even daily fluxes of normal magnitude (up 20g of CO₂ /m²/d for daily fluxes see Chapter 3) for a grassland site can lead to an important net uptake of carbon when summed up in respect of time. Nitrogen fertilizers highly spread on the site can accentuate this trend. The period when the site behaves as a source of CO₂ is therefore shorter than usually observed for similar vegetation with other climates. Another issue that have been raised here is the use of the site by cattle and the effects of the silage cuts. Those two activities removed from the site organic matter that would have decayed and released CO₂. They stimulated the growth as well by bringing more light to the most active and youngest grass situated near the ground. In the mean time the LAI is reduced and so is the photosynthetic flux. A better understanding of those processes is required.

As for the modelling part of this study, both models used here give acceptably results and seem to describe well physical and biological reality. Jacobs' model shows a better response to the seasonality of carbon dioxide fluxes, but has some instability problems. Collatz's model depicts very accurately the photosynthesis process over the year, especially the cumulated photosynthesis over the study period. However, both models predict a shorter source period for the site than observed and a lag effect for the timing of maximum uptake and maximum release. For all time steps studied in chapter 4, the autumnal decrease in CO₂ flux and the spring increase are not close to the observations. Those transition periods are especially hard to model, but should be improved by a better analysis of the LAI behaviour of the vegetation. Indeed, the modelling work performed here can be considered as the first step for further study since it has been calibrated with a constant LAI.

5.2 Suggestion for further investigation

The modelling principle has many applications. In the future, some measurements on the site of the leaf area index should improve our knowledge of the growth of plants throughout seasons, highlight the effects of silage cuts on grass growth and give a good assessment of the amount of matter removed in summer. Such measurements are widely described in the literature and could be either carried out by remote sensing measurements (from satellite data) or with manual measurements as it is usually done for sites of field scale size such as our catchment. This data could then be used to validate a model of growth to simulate a variable LAI during the year. Such modules have already been tested by Calvet *et al.* (2000), Mougín *et al.* (1995) or Ji *et al.* (1995). They depend only on two constant variables and are therefore easily adaptable to any conditions. The main input is the biomass and can be calculated from

any assimilation model. A further step ahead is to consider the effect of climate change. For those conditions, the growth module needs to be modified. The two variables held constant for a given environment should be changeable (see Calvet *et al.*, 2000). To do so nitrogen content of plants needs to be known (Dewar, 1996).

Another task for future research is to couple the semi-empirical models of CO₂ flux described here within a Soil Vegetation Atmosphere Transfer (SVAT) scheme. The SVAT thus obtained allows a more realistic description of the canopy stomatal conductance and the estimated assimilation rate is used to both simulate plant growth and diagnose a leaf area index consistent with the climate and the atmospheric CO₂ concentration. This has been done by Calvet *et al.* (1998) from the SVAT model ISBA and the A-gs described by Jacobs model. From the water balance point of view, a better stomatal conductance definition and the impact of increasing ambient CO₂ concentration affect directly the transpiration from plant. Such a modelling effort could then examine climate scenarios (such as increased precipitation).

Finally, it can be noticed that in this study, only two components are considered in the CO₂ fluxes: the ecosystem respiration (nighttime CO₂ flux) and the photosynthesis (daytime CO₂ flux minus the daytime CO₂ respiration deduced from the nighttime measurements). However, the soil surface carbon dioxide flux, the sum of plant root and microbial respiration, is an important part of the carbon cycle of terrestrial ecosystem too. In our case no device measured this component alone, so that it could not be separated from the plant respiration (they together compose the ecosystem respiration). Many papers report the method of close-chamber or open-chamber measurements, used to measure soil respiration, and the accuracy of such a device (Iritz *et al.*, 1997). This could be an interesting part to add to the instruments present on this Irish grassland site to deepen the understanding of processes at stake for the carbon budget.

Bibliography

Bibliography

- Baldocchi, D.D., Valentini, R., Running, S.R., Oechel, W., Dahlman, R., 1996. Strategies for measuring and modeling carbon dioxide and water fluxes over terrestrial ecosystems. *Global Change Biol.* 2, 159-168.
- Ball, J.T., Woodrow, I.E., Berry, J.A., 1987. A model predicting stomatal conductance and its contribution to the control of Photosynthesis under different environmental conditions. *Progress in Photosynthesis Research.* 4, 221-224.
- Berry, J.A., Raison, J.K., 1982. Responses of Macrophytes to temperature. In: Lange, O.L., Nobel, P.S., Osmond, C.B., Ziegler, H., *Encyclopedia of Plant Physiology, New series, Vol. 12B, Physiological Plant Ecology II.* Springer Verlag, Berlin, 277-338.
- Bruse, M., 2001. ENVI-met implementation of the Jacobs A-gs model to calculate the stomata conductance. Working paper.
- Calvet, J.C., Noilhan, J., Roujean, J.L., Bessemoulin, P., Cabelguenne, M., Olioso, A., Wigneron, J.P., 1998. An interactive vegetation SVAT model tested against data from six contrasting sites. *Agric. For. Meteorol.* 92, 73-95.
- Calvet, J.C., Soussana, J.F., 2001. Modelling CO₂ enrichment effects using an interactive vegetation SVAT scheme. *Agric. For. Meteorol.* 108, 129-152.
- Campbell, G.S., Norman, J.M. An introduction to environmental biophysics. Second Edition
- Collatz, G.J., Ball, J.T., Grivet, C., Berry, J.A., 1991. Physiological and environmental regulation of stomatal conductance, photosynthesis and transpiration: a model that includes a laminar boundary layer. *Agric. For. Meteorol.* 54, 107-136.
- Collatz, G.J., Ribas-Carbo, M., Ball, J.A., 1992. Coupled photosynthesis-stomatal conductance model for leaves of C₄ plants. *Aust. J. Plant Physiol.* 19, 519-538.
- Cook, F.J., Thomas, S.M., Kelliher, F.M., Whitehead, D., 1998. A model of one-dimensionnal steady-state carbon dioxide diffusion from soil. *Ecol. Model.* 109, 155-164.
- Dagnelie, P., 1991. *Théorie et Méthodes Statistiques, Vol. 1.* Presses Agronomiques de Gembloux, Gembloux, Belgium.
- Dewar, R.C., 1996. The correlation between plant growth and intercepted radiation: an interpretation in terms of optimal plant Nitrogen content. *Annals of Botany,* 78, 125-136.
- Dugas, W.A., Heuer, M.L., Mayeux, H.S., 1999. Carbon dioxide fluxes over a Bermuda grass, native prairie, and sorghum. *Agric. For. Meteorol.* 93, 121-139.

Bibliography

- Falge, E., Baldocchi, D.D., Olson, R., et al., 2001. Gap filling strategies for defensible annual sums of net ecosystem exchange. *Agric. For. Meteorol.* 107, 43-69.
- Farquhar, G.D., von Caemmerer, S., Berry, J. A., 1980. A biochemical model of photosynthetic CO₂ assimilation in leaves of C₃ species. *Planta.* 149, 78-90.
- Frank, A.B., Dugas, W.A., 2001. CO₂ fluxes over a northern semiarid mixed grass prairie. *Agric. For. Meteorol.* 108, 317-326.
- Goudriaan, J., van Laar, H.H., van Keulen, H., Lovworse, W., 1985. Photosynthesis, CO₂ and plant production. In: Day, W. Day & R.K. Atkin (Eds.), *Wheat growth and modelling*. NATO ASI Series, Series A, Vol. 86. Plenum Press, New York, 107-122.
- Goulden, M.L., Munger, J.W., Fan, S.M., Daube, B.C., Wofsy, S.C., 1996. Measurements of carbon sequestration by long-term eddy covariance: methods and critical evaluation of accuracy. *Global Change Biol.* 2, 169-182.
- Ham, J.M., Knapp, A.K., 1998. Fluxes of CO₂, water vapor and energy from a prairie ecosystem during the seasonal transition from sink to carbon source. *Agric. For. Meteorol.* 89, 1-14.
- Haszpra, L., Barcza, Z., Bakwin, P.S., Berger, B.W., Davis, K.J., Weidinger, T., 2001. Measuring system for the long-term monitoring of biosphere/atmosphere exchange of carbon dioxide. *J. Geophys. Res.* 106, 3057-3069.
- Hensen, A., Vermeulen, A.T., Wyers, G.P., Zhang, Y., 1996. Eddy correlation and relaxed eddy accumulation measurements of CO₂ fluxes over grassland. *Phys. Chem. Earth*, 21, 383-388.
- Houghton, J., 1990. *Global climate change digest report*.
- Iritz, Z., Lindroth, A., Gardenas, A., 1997. Open ventilated chamber system for measurements of H₂O and CO₂ fluxes from the soil surface. *Soil technology.* 10, 169-184.
- Jacobs, C.M.J., 1994. Direct impact of atmospheric CO₂ enrichment on regional transpiration. Ph.D. Thesis. Agricultural University, Wageningen.
- Jarvis, P.G., 1976. The interpretation of leaf water potential and stomatal conductance found in canopies in the field. *Phil. Trans. R. Soc. London B.* 273, 593-610.
- Katul, G.G., Ellsworth, D.S., Lai, C.T., 2000. Modelling assimilation and intercellular CO₂ from measured conductance : a synthesis of approaches. *Plant, Cell, Environ.* 23, 1313-1328.
- Lai, C.-T., Katul, G., Butnor, J., Ellsworth, D., Oren, R., 2002. Modelling night-time ecosystem respiration by a constrained source optimization method. *GlobalChange Biology*, 8, 124-141.

Bibliography

- Leuning, R., 1995. A critical appraisal of a combined stomatal-photosynthesis model for C3 plants. *Plant, Cell Environ.* 18, 339-355.
- Lhomme, J.P., 2001. Stomatal control of transpiration : examination of the Jarvis-type representation of canopy resistance in relation to humidity. *Water Resour. Res.* 37, 689-699.
- Lloyd, J., Taylor, J.A., 1994. On the temperature dependence of soil respiration. *Funct. Ecol.* 8, 315-323.
- Meidner, H., Mansfield, T.A., 1968. *Physiology of Stomata*, McGraw-Hill, London.
- Michaelis, L., Menten, M.L., 1913. Die Kinetik der Invertinwirkung. *Biochem. Z.* 49, 333.
- Mielnick, P.C., Dugas, W.A., 2000. Soil CO₂ flux in a tallgrass prairie. *Soil Biology & Biochemistry.* 32, 221-228.
- Moncrieff, J.B., Mahli, Y., Leuning, R., 1996. The propagation of errors in long term measurements of land atmosphere fluxes of carbon and water. *Global Change Biol.* 2, 231-240.
- Moncrieff, J.B., Massheder, J.M., de Bruin, H., Elbers, J., Friborg, T., Heusinkveld, B., Kabat, P., Sctt, S., Soegaars, H., Verhoef, A., 1997. A system to measure surface fluxes of momentum,
- Pachepsky, L.B., Haskett, J.D., Acock, B., 1996. An adequate model of photosynthesis . I : Parameterisation, validation and comparison of models. *Agricultural Systems.* 50, 209-225.
- Pachepsky, L.B., Acock, B., 1996. An adequate model of photosynthesis . II : Dependence of parameters on environmental factors. *Agricultural Systems.* 50, 227-238.
- Osborne, C.P., Woodward, F.I., 1999. *The MEDRUSH Vegetation*
- Ruimy, A., Jarvis, P.G., Baldocchi, D.D., Saugier, B., 1995. CO₂ fluxes over plant canopies and solar radiation: a review. *Adv. Ecol. Res.* 26, 1-63.
- Saigusa, N., Oikawa, T., Liu, S., 1998. Seasonal variations of the exchange of CO₂ and H₂O between a grassland and the atmosphere: An experimental study. *Agric. For. Meteorol.* 89, 131-139.
- Schmid, H.P., Grimmond, C.S.B. Cropley, F., Offerle, B., Su, H.B., 2000. Measurements of CO₂ and energy fluxes over a mixed hardwood forest in the mid-western United States. *Agric. For. Meteorol.* 103, 357-374.
- Sims, P.L., Bradford, J.A., 2001. Carbon dioxide fluxes in a southern plains prairie. *Agric. For. Meteorol.* 109, 117-134.

Bibliography

- Smith, E., 1938. Limiting factors in photosynthesis: light and carbon dioxide. *Gen. Physiol.* 22, 21–35.
- Svejcar, T.J., Browning, J.A., 1988. Growth and gas exchange of *Andropogon gerardii* as influenced by burning. *J. Range Manage.* 41, 239-244.
- Valentini, R., Matteucci, G., Dolman, A.J., Schulze, E.-D., Rebmann, C., Moors, E.J., Granier, A., Gross, P., Jensen, N.O., Pilegaard, K., Lindroth, A., Grelle, A., Bernhofer, C., Grünwald, T., Aubinet, M., Ceulemans, R., Kowalski, A.S., Vesala, T., Rannik, Ü., Berbigier, P., Loustau, D., Gu g mundsson, J., Thorgeirsson, H., Ibrom, A., Morgenstern, K., Clement, R., Moncrieff, J., Montagnani, L., Minerbi, S., Jarvis, P.G., 2000. Respiration as the main determinant of carbon balance in European forests. *Nature* 404, 861–865.
- Verhoef, A., Allen, S.J., 2000. A SVAT scheme describing energy and CO₂ fluxes for multi-component vegetation : calibration and test for a Sahelian savannah. *Ecol. Model.* 127, 245-267.
- Vourlitis, G.L., Oechel, W.C., 1999. Eddy covariance measurements of CO₂ and energy fluxes of an Alaskan tussock tundra ecosystem. *Ecology*, 80, 686-701.
- Webb, E.K., Pearman, G.I., Leuning, R., 1980. Correction of flux measurements for density effects due to heat and water vapor transfer. *Quart. J. R. Meteorol. Soc.* 106, 85-100.
- Xu, L.K., Matista, A.A., Hsiao, T.C., 1999. A technique for measuring CO₂ and water vapor profiles within and above plant canopies over short periods. *Agric. For. Meteorol.* 94, 1-12.

Appendix 1

Appendix 1

Notation	Description	Value	Units	Source
A_g	gross assimilation rate	Equ(4.9) Equ(4.4)	$\mu\text{mol}/\text{m}^2/\text{s}$	Collatz Jacobs
A_m	the photosynthetic rate at light saturation	Equ(4.20)	$\text{mg}/\text{m}^2/\text{s}$	
$A_{m_max}(@25)$	maximum value for A_m @ 25 °C	2.4	$\text{mg}/\text{m}^2/\text{s}$	
A_n	Net assimilation	Equ(4.10) Equ(4.19)	$\mu\text{mol}/\text{m}^2/\text{s}$	Collatz Jacobs
b_{gs}	intercept in B-B model	0.003	$\text{mol}/\text{m}^2/\text{s}$	Ball-Berry
C_a	ambient CO_2 conc	380	ppm	
C_{i_min}	minimum C_i when stomata are closed from water stress	190	ppm	Farquhar
C_o	oxygen concentration in air	210000 air	$\mu\text{mol}/\text{mol}$	
C_p		1005	$\text{J}/\text{kg air}/\text{C}$	
D_{max}	maximum vapor pressure deficit	45	g/kg	Jacobs
D_s	vapor pressure deficit	$1000(q_{asat} - q_a)$	g/kg	Jacobs
e_m	maximum moles CO_2 fixed per quantum PAR	0.08	$\text{mol}/\text{quantum}$	Farquhar
f_o	f factor value for $D_s=0\text{g}/\text{k}$	0.85 0.94	unit less	Jacobs This case
g_c	cuticular conductance	0.25	mm/s	
$g_m(@25)$	mesophyll conductance @ 25°C	7.0	mm/s	

Appendix 1

Notation	Description	Value	Units	Source
g_s	Stomatal conductance for water vapor	Equ(4.14) Equ(4.30)	mol/m ² /s mm/s	Collatz Jacobs
g_{sc}	Stomatal conductance for CO ₂	Equ(4.28)	mm/s	
h_s	humidity @ leaf surface		decimal fraction	
J_c	Rubisco-limited rate	Equ(4.7)	μmol/m ² /s	Collatz
J_e	Light-limited rate	Equ(4.6)	μmol/m ² /s	Collatz
$J_{max}(@25)$	light saturated potential rate of electron @ 25 ° C	210	μEq/m ² /s	Farquhar
J_s	Sucrose-limited rate	Equ(4.8)	μmol/m ² /s	Collatz
k	stefan boltzmann constant	5.67e-8		
$K_c(@25)$	Michaelis constant for CO ₂ fixation at @ 25°C	460	μmol/mol	Farquhar
$K_o(@25)$	Michaelis constant for O ₂ fixation at @ 25°C	330000	μmol/mol	Farquhar
lai	Leaf area index	1.5		This case
L_v		2450	J/gH ₂ O	
m	Ball-Berry constant	5.6 6.75		Ball-Berry This case
m_{air}	molecular weight of air	28.97	g/mol	
m_c	molecular weight of carbon dioxide	44.0098	g/mol	
M_c	molecular weight of carbon	12	g/mol	
m_v	molecular weight of water	18.02	g/mol	
P	atmospheric pressure	1013	mb	

Appendix 1

Notation	Description	Value	Units	Source
$q(\tau)$	temperature coefficient for τ	-0.041 -0.056 -0.02	unit less	Farquhar Collatz (C ₄ grass) This case
$q(J_{max})$	temperature coefficient for J_{max}	0.0524	unit less	Farquhar
$q(K_c)$	temperature coefficient for K_c	0.084 0.074 0.07	unit less	Farquhar Collatz (C ₄ grass) This case
$q(K_o)$	temperature coefficient for K_o	0.051 0.018 0.05	unit less	Farquhar Collatz (C ₄ grass) This case
$q(R_d)$	temp coeff for R_d	0.094	unit less	Farquhar
$Q_{10}(\Gamma)$	Q_{10} coefficient for Γ	1.5 1.2	unit less	Jacobs This case
$Q_{10}(A_{m,max})$	Q_{10} coefficient for $A_{m,max}$	2 1.6	unit less	Jacobs This case
$Q_{10}(g_m)$	Q_{10} coefficient for g_m	2 1.6	unit less	Jacobs This case
q_a	specific air humidity		kg/kg	
R_{gas}	universal gas constant	8.314	J/mol/K	
R_a	gas constant for air	287.05	J/kg/K	
$R_d(@25)$	$0.015 * V_m(@25)$	1.1	$\mu\text{mol}/\text{m}^2/\text{s}$	Farquhar
R_v	gas constant for vapour pressure	461.51	J/kg/K	
$V_m(@25)$	maximum carboxylation velocity at @ 25°C	98	$\mu\text{mol}/\text{m}^2/\text{s}$	Farquhar
α_{PAR}	leaf absorptivity	0.8		Farquhar

Appendix 1

Notation	Description	Value	Units	Source
$\Gamma(@25)$	compensation point @ 25°C	45	ppm	Jacobs
ϵ_o	maximum quantum use efficiency	0.017	mg/J	Jacobs
ρ	superficial density of chlorophyll	0.45	g/m ²	
ρ_a	density of air		kg/kg	
ρ_g	molar density of any gases	44.6	mol/m ³	
ρ_v	density of water	1e6	g/m ³	
$\tau(@25)$	Ratio of partitioning between carboxylase and oxigenase reactions of Rubisco	3416		Farquhar
φ_c	conversion factor transforming [CO2]	Equ(4.21)	from ppm into mg/m ³	Jacobs

Appendix 2.1:
Collatz's model
Matlab Codes

```

%=====
%                               Collatz's model
%=====

%----- humidity parameters-----

easat=6.112*exp(17.67.*(ta2-273.15)/(ta2-29.65));
% hectapascals (same as millibars)
%ta2 is the air temperature in deg. K.
%ta1 is the air temperature in deg. C.

qasat=0.622*easat./(patm-.378*easat);
% density of water vapour at saturation/density of dry air at saturation
qa=(rh./100).*qasat;
% Specific air humidity <kg/kg>

%-----PAR flux and LAI-----

lai=1.5;
Q=Qtot.*(1+exp(-0.4*lai))./2;

%-----Constants-----

alphapar=0.8;
%leaf absorptivity
Co=210000;
%oxygen concentration in air in <micromol/mol>
Cimin=190;
%minimum Ci when stomata are closed from water stress
Ca=380;
%ambient CO2 concentration in <ppm>
em=0.08;
%maximum moles CO2 fixed per quantum PAR
Jmax25=210;
%light saturated potential rate of electron @ 25 deg C <microEq/m^2/s>
Ko25=330000;
%Ko @ 25 deg in <micromol/mol>
Kc25=460;
%Kc @ 25 deg in <micromol/mol>
rau=0.45;
%superficial density of chlorophyll in <g/m^2>
tau25=3416;
%tau @ 25 deg C =Ko25*kc/(ko*Kc25)Vm25=98
Ko_tcoeff=0.051;
Kc_tcoeff=0.07;
tau_tcoeff=-0.02;
m=6.75;
%intercept in B-B model
b_gs=0.003;
%intercept in B-B model in <mol/m2/s>
hs=rh./100; %humidity @ leaf surface
%in decimal fraction
Cs=Ca;

%-----Temperature dependent parameter-----

Vm=Vm25.*exp(8.8*10^(-2).*(ta1-25))./(1+exp((ta1-41).*0.29));
%Rubisco capacity needs high temperature cut off
Rd=Rd25.*exp(0.069.*(ta1-25))./(1+exp((ta1-55).*1.3));
%leaf respiration rate needs high temperature cut off
Jmax=0.45*483.*exp(-37000.*(ta2-298))./(8.314.*ta2.*298))./(1 + exp((710.*ta2 -
220000))./(8.314.*ta2)));
tau=tau25.*exp(tau_tcoeff.*(ta1-25));
%ratio of RuBP used by carboxylase or oxygenase activity with Rubisco

```

```

gamma2=Co./(2.*tau);
                                %<micromol/mol> CO2 compensation point (min Ci for finite A)
Ko=Ko25.*exp(Ko_tcoeff.*(ta1-25));                                %Michaelis for O2
Kc=Kc25.*exp(Kc_tcoeff.*(ta1-25));                                %Michaelis constant for CO2

%-----Net assimilation-----

Ci(1)=342;

for i = 1:nt

Je(i)=alphapar*em*Q(i)*(Ci(i)-gamma2(i))/(Ci(i)+2*gamma2(i));
                                %light-limited assimilation rate

    if Je(i) > Jmax
        Je(i)=Jmax ;
    end

Jc(i)=Vm(i)*(Ci(i)-gamma2(i))/(Ci(i) + Kc(i)*(1+Co/Ko(i)));
                                %Rubisco-limited assimilation rate
Js(i)=Vm(i)/2;                                %sucrose-limited assimilation rate
Ao(i)=min([Je(i) Jc(i)]);
Ao(i)=min([Ao(i) Js(i)]);
Anet(i)=Ao(i) - Rd(i);                                %net carbon assimilation

%-----Ball Berry Model-----

gs(i)=m*Anet(i)*hs(i)/Cs + b_gs;                                %<mol/m2/s>

%-----Fick's Law of Diffusion-----

Ci(i+1)= Ca - Anet(i)/gs(i);

    if Ci(i+1) < Cimin
        Ci(i+1)=Cimin;
    end

    if Q<=0                                %controls conditions of low light when respiration elevates Ci
        Ci(i+1)=Ca + 10;
    end

end

```

Appendix 2.2:
Jacobs' model
Matlab Codes

```

%=====
%                               Jacobs model
%=====

%----- humidity parameters-----

easat=6.112*exp(17.67.*(ta2-273.15)./(ta2-29.65));
% hectapascals (same as millibars)
%ta2 is the air temperature in deg. K.
%ta1 is the air temperature in deg. C.

qasat=0.622*easat./(patm-.378*easat);
% density of water vapour at saturation/density of dry air at saturation
qa=(rh./100).*qasat;
% Specific air humidity <g/kg>

%-----PAR flux and LAI-----

lai=1.5;
Q=Qtot.*(1+exp(-0.4*lai))./2;

%-----Constants-----

Am_max25=2.4000;
Ca=380;
Ds=qasat.*1000-qa.*1000;
Dmax=45;
eps0=0.017;
gc=0.25;
gm25=7.0;
gamma25=45;
f0=0.94;
Q10_gamma=1.2;
Q10_Am_max=1.6;
Q10_gm=1.6000;
Ra=287.05;
Rv=461.51;
raua=patm.*10^2./(Ra.*ta2.*(1+(Rv/Ra-1).*qa./1000));
phic=mc.*raua./mair;

Am_max25 %maximum value for Am @ 25 deg C in <mg/m^2/s>
Ca %ambient CO2 conc, in <ppm>
Ds %vapor pressure deficit in <g/kg>
Dmax %maximum vapor pressure deficit in <g/kg>
eps0 %maximum quantum use efficiency in <mg/J>
gc %cuticular conductance in <mm/s>
gm25 %mesophyll conductance @ 25 deg C in <mm/s>
gamma25 %compensation point @ 25 deg C
f0 %f factor value for Ds=0g/kg <unitless>
Ra %gas constant for air in <J/kg/K>
Rv %gas constant for vapour pressure in <J/kg/K>
raua %density of air in kg/kg>
phic %conversion factor transforming [CO2]from <ppm> into <mg/m^3>

%-----Temperature dependent parameters-----

gm=gm25.*Q10_gm.^((ta1-25)./10)./((1 + exp(0.3.*(5-ta1))).*(1 + exp(0.3.*(ta1-28))));
fmin=gc./(gc + gm);
gamma=gamma25.*Q10_gamma.^((ta1-25)./10);
Cmin=(gc.*Ca + gm.*gamma)./(gm + gc);
Am_max=Am_max25.*Q10_Am_max.^((ta1-25)./10)./((1 + exp(0.3.*(8-ta1))).*(1 + exp(0.3.*(ta1-38))));
%for Ds=Dmax in <ppm>

```

```

%-----Internal [CO2] Ci-----
f=f0.*(1- Ds./Dmax) + fmin.*Ds./Dmax;
Ci=f.*Ca + (1-f).*gamma;

%-----Net assimilation-----

eps=eps0.*(Ci - gamma)/(Ci + 2.*gamma);
Am=Am_max.*(1 - exp((-0.001.*gm.*(Ci - gamma).*phic)/Am_max));
Rd=Am./9;                                     %respiration
An=(Am + Rd).(1 - exp((-eps.*Q)/(Am + Rd)))-Rd; %<mg/m2/s>

%-----Estimating the stomatal response-----

Ag= An + Rd;
Am_g= Am + Rd;
Amin= 0.001.*gm.*(Cmin - gamma).*phic;

gsc=(An - Amin.*Ds.*Ag/(Dmax.*Am_g) + Rd.*(1-Ag./Am_g))/((Ca -Ci).*phic);
%conductance of the leaf to CO2
gs=1.6*1000.*gsc + gc;                       %stomatal conductance for water vapor in <mm/s>

```

Appendix 3
Complementary Production

EGS conference April 2002, Nice:

At the occasion of the EGS (European Geophysical Society) conference 2002 in Nice, a poster has been elaborated in collaboration with Yan Lacaze. Several formulations for surface runoff, subsurface runoff, diffusion, drainage and base-flow, adapted from recent SVAT models (ISBA, SEWAB, LAPS) have been added to the initial model (Noihlan et al. 1989) adapted for Dripsey site by J. Albertson and G. Kiely (Journal of Hydrology (2001)).

Hereunder are joined the submitted abstract as well as the complete poster.

Abstract:

A COMPARISON OF 2, 3 AND 4 LAYERS SOIL MODELS WITHIN A SVAT SCHEME FOR THE WATER BALANCE OF A SMALL IRISH GRASSLAND SITE.

Y. Lacaze (1), C. Le Bris (1), J. Albertson(2), G. Kiely(1)

(1) Dept. of Civil and Environmental Engineering, University College, Cork, Ireland

(2) Dept. of Civil and Environmental Engineering, Duke University, NC, USA

In recent years, the knowledge of transfers of water and heat between the soil, vegetation, and atmosphere is improving. Soil-Vegetation-Atmosphere Transfers (SVAT) modelling simulate well some variables dealing specially with the water balance, such as evaporation and soil moisture. In order to assess the impact of the number of soil layers defined in the models, we have used several formulations for surface runoff, subsurface runoff, diffusion, drainage and base-flow, adapted from recent SVAT models (ISBA, SEWAB, LAPS). A two-layer soil hydrological configuration developed by Albertson and Kiely (Journal of Hydrology (2001)) was used as a basis for the different schemes. The ISBA model (Noilhan et al. 1999) has been used as a first attempt for the water budget. We have improved the results by adding a third soil layer as advocated by A. Boone et al. (1999). In parallel with that, we tested the SEWAB model (Mengelkamp et al. 1999) and the LAPS model (Mihailović 1996) in their three-layer and multi-layer soil configurations. The outputs have been compared with data collected at a small grassland site near Cork, Ireland. The use of a third soil layer improves the simulation of the hydrological processes compared to a two-layer soil model. However computing with more than three layers does not improve the accuracy of the simulation and a further disadvantage is increased complexity.

Poster: (see end of the thesis)

AGU conference December 2002, San Francisco:

At the occasion of the AGU (American Geophysical Union) conference in December 2002 in San Francisco, an abstract has been submitted on the present thesis.

Abstract:

Observations and Modelling of Carbon Dioxide flux from a Highly Nitrogen Fertilized Irish Grassland

CHARLOTTE LE BRIS (1), GERARD KIELY (1)

¹ *Dept. of Civil and Environmental Engineering, University College, Cork, Ireland*

Seasonal variations in the CO₂ flux were investigated and modelled over a grassland in South West Ireland. The climate is temperate and humid with mean annual precipitation of about 1400 mm for the area. The grassland type can be described as moderately high quality pasture and meadow classified into the C₃-grass category. Data were recorded continuously at 30 minutes intervals by an aerodynamic method for one full year, between the 3rd of July 2001 and the 3rd of July 2002. The grassland absorbed CO₂ during the periods from July to September 2001 and from February to July for 2002. The maximum daily net ecosystem CO₂ exchange during the growing period was up to 20 g of CO₂ m⁻² day⁻¹ and the net uptake for the whole period was 3.8 T of Carbon. Those results are compared with CO₂ fluxes for grasslands for other countries with different climates and land use management.

Two semi-empirical models were then applied to simulate the net ecosystem CO₂ flux different time steps. The model proposed by Collatz *et al* (1991) considers the full biochemical components of photosynthetic carbon assimilation from Farquhar *et al.* (1980), and an empirical model of stomata conductance from Ball *et al.* (1987). The model proposed by Jacobs (1994) is based on the empirical model of stomatal conductance from Jarvis (1976), and on a less detailed assimilation model from Goudriaan *et al.* (1985). Both models satisfactorily predict CO₂ fluxes over the seasons for the grass catchment.

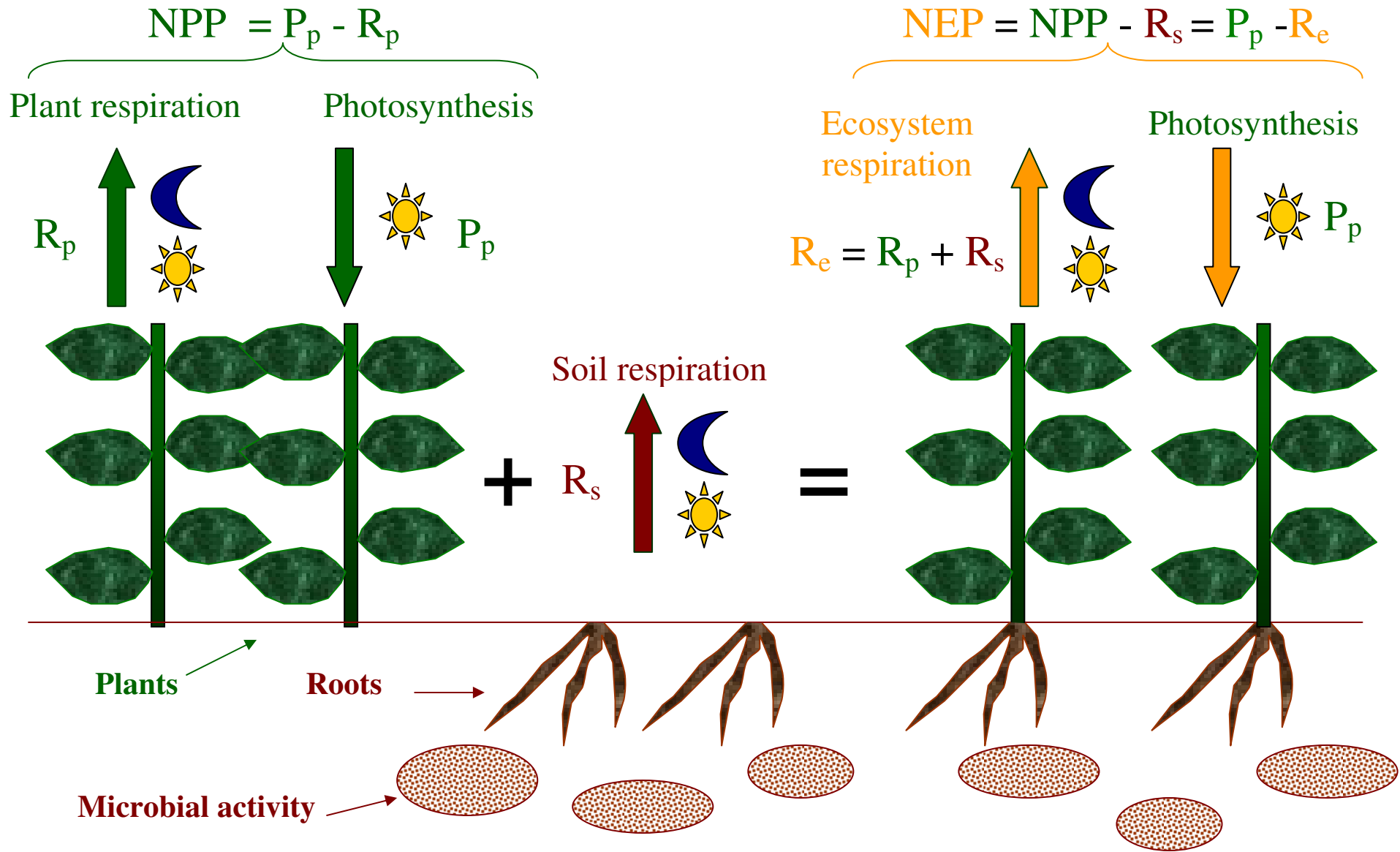


Figure 4.1.2: CO₂ budget